

## CHAPTER 3

# INTEGRATION BETWEEN TEMPLATE-BASED NANOSTRUCTURED SURFACES AND BIOSENSORS

*Walter Vastarella<sup>1\*</sup>, Jan Maly<sup>2</sup>, Mihaela Ilie<sup>3</sup>, Roberto Pilloton<sup>1</sup>*

\*corresponding author: [walter.vastarella@casaccia.enea.it](mailto:walter.vastarella@casaccia.enea.it)

<sup>1</sup> ENEA C.R. Casaccia, Via Anguillarese 301, 00123- S. Maria di Galeria, Rome (ITALY)

tel. ++390630484096 fax. ++390630486591

[www.biosensing.net](http://www.biosensing.net)

<sup>2</sup> *Dep. of Biology, University of J.E.Purkyne, 40001 Usti nad Labem (CZECH REP.)*

<sup>3</sup> *Dept. of Applied Electronics and Information Engineering, faculty of Electronics,  
Telecommunications and Information technology, LAPI, Univ. 'Politehnica' Bucuresti, Bd.  
Iuliu Maniu nr. 1-3, sector 6, Bucharest (ROMANIA)*

## ABSTRACT

Nanostructured materials have attracted considerable attention in many fields of science, for their extremely peculiar properties due to the down-scaling. Amongst the large number of nanomaterials applications in biosensing and bioanalytical techniques, this chapter is focused on the modification of sensitive surfaces with nanostructured materials (namely nanosphere and nanowires) produced by means of templates. The main subjects are nano or micro-sphere lithography for biosensing applications and electrochemical biosensors based on metal nanowires or fibres, with a special attention to their sensitivity and extended applicability range.

**Keywords:** *nanosphere lithography, porous template, nanoelectrode ensemble, addressed immobilization*

### Abbreviations list

**AFM:** atomic force microscopy; **BSA:** bovine serum albumin; **CV:** cyclic voltammetry; **CYS:** cysteamine; **EDM:** electrochemically deposited multilayers; **FIA:** flow injection analysis; **GA:** glutaraldehyde; **GOx:** glucose oxidase; **LOD:** limits of detection; **LSPR:** localized surface plasmon resonance; **NEEs:** nanoelectrode ensembles; **NEE/SPS:** nanoelectrode ensemble on screen printed substrate; **NSL:** nano-sphere lithography; **NTA:** nitrilotriacetic; **PAA:** polymerized acrylic acid; **PANI:** polyaniline; **PBS:** phosphate buffer solution; **PC:** polycarbonate; **PE-CVD:** plasma enhanced chemical vapour deposition; **PEG or PEO:** poly(ethylene)glycol; **PMMA:** poly(methyl methacrylate); **PS:** polystyrene; **QCM:** quartz crystal microbalance; **RE:** reference electrode; **RF:** radio frequency; **RIE:** reactive ion etching; **SAM:** self-assembled monolayer; **SEM:** scanning electron microscopy; **SPE:** screen printed electrode; **TEM:** transmission electron microscopy; **WE:** working electrode; **μCPS:** micro contact particle stripping; **μCP:** micro contact printing.

## CHAPTER'S CONTENT

3.1- INTRODUCTION	p. 5
3.2- NANOSPHERE LITHOGRAPHY	
3.2.1- Basic principles of nanosphere lithography (NSL)	p. 6
3.2.2- Preparation of colloidal mask	p. 8
3.2.3- Plasma modifications and lithography	p. 11
3.2.4- Combination of NSL and other lithographic approaches	p. 13
3.2.5- Application of NSL for sensor biointerfaces	p. 15
3.2.5.1 <i>Biointerfaces based on protein nanoarrays</i>	p. 15
3.2.5.2 <i>Biointerfaces for localized surface plasmon resonance biosensors</i>	p. 20
3.3- NANO-ELECTRODES ENSEMBLE FOR BIOSENSING DEVICES	
3.3.1- Electrochemical and electroless deposition of nanomaterials via templates	p. 25
3.3.1.1- <i>Nanoporous membranes</i>	p. 25
3.3.1.2- <i>Deposition of metals in porous templates</i>	p. 28
3.3.1.3- <i>Characterization of nanomaterials in porous templates</i>	p. 31
3.3.2- Gold nanoelectrode ensembles	p. 32
3.3.2.1- <i>Morphological features of gold Nanoelectrode Ensembles</i>	p. 34
3.3.2.2- <i>Electrochemical features of gold Nanoelectrode Ensembles</i>	p. 35
3.3.2.3- <i>Deposition of Nanoelectrode Ensembles on substrates</i>	p. 38
3.3.3- Nanoelectrode ensemble for enzyme based biosensors	p. 40
3.3.3.1- <i>State of the art</i>	p. 40
3.3.3.2- <i>Nanoelectrode ensemble on screen printed based biosensors</i>	p. 42

3.3.3.3- <i>Analytical performances of NEE/SPS based biosensors</i>	p. 45
3.3.4- Concluding remarks	p. 48
REFERENCES	p. 57

# INTEGRATION BETWEEN TEMPLATE-BASED NANOSTRUCTURED SURFACES AND BIOSENSORS

*Walter Vastarella, Jan Maly, Mihaela Ilie, Roberto Pilloton*

## 3.1 Introduction

Nanostructured materials have proven to be a powerful tool in new technologies as well as in basic research, due to their very peculiar properties at nanometer size scale. Many studies and publications have demonstrated, or are based on the assumption that, optical, mechanical, photo-catalytic or electronic properties of the nanosized surfaces drastically changes with respect to those of the bulk materials [1-22]. Electrochemical sensing and biosensing constitute research fields where nanotechnologies have been successfully applied, especially in using metal and carbon nanosized materials with high surface to volume ratio [9-14].

The synthesis via template represents a convenient procedure which in many cases has strongly simplified the production of surface confined nanoscale materials as nanoparticles, nanowires or nanotubes. This method is essentially based on the simple but effective idea that the pores or cavities of the host supports can be used as templates to address and control the growth of specific materials, i.e. metals, semiconductors, biological compounds and polymer chains.

The utilization of templates in producing novel nanomaterials goes back to the early eighties. Pioneering works were ascribed to authors involved in the preparation of

different metallic nanostructures [23-40], but presently the method was extended to a large number of substrates and applications.

This chapter is focused on the following nanomaterials which rely on template synthesis: nanostructured ordered surfaces prepared by nano-sphere lithography (NSL), and metal nanoelectrode ensembles (NEEs) produced into porous membranes. Apart from theoretical approach, the attention here is paid to the integration of nanoelectrode ensembles with disposable screen printed devices, which represent an interesting example of practical application for biosensing. Features and advantages of such devices, with respect to comparable macroscopic systems, are described and future perspectives are finally suggested.

## **3.2 Nanosphere lithography**

### ***3.2.1 Basic principles of nanosphere lithography***

The major issue in the development of nanoscale ordered biointerfaces is the way of precise positioning of nano-objects in periodic or aperiodic patterns. A nanostructured biointerface is usually obtained by selective anchoring of biomolecules through chemical bounds to nanopatterned substrate. Apart from conventional patterning techniques (e.g. electron beam lithography), such substrates can be conveniently prepared by low-cost alternative technique called **nano-sphere lithography (NSL)**. This technique make use of self-assembling processes of nanometer-scale spherical particles onto a large area of planar substrate followed by several different steps of plasma etching and deposition processes, creating in this way polymeric or metallic

nano-structures with relevant applications to bio-interfaces. This “bottom-up” method is rather old, originally developed as a “natural lithography” technique for replicating submicroscopic patterns [41]. Recently, it has undergone a rapid development showing many applications in various fields where large numbers of periodical nano-sized features are often required, such as nanopattern definition in a variety of biological investigations like cell adhesion studies [42-46], fabrication of nanostructured biointerfaces for bioanalytical devices (biosensors) [47-50] and preparation of catalytically active surfaces [51,52]. The main advantages of the method, which are the driving force of its development, are the ability to independently control the size, shape and coverage of particles over large areas ( $\text{cm}^2$ ), the low-cost and simplicity of preparation without need of costly equipment and strict conditions (e.g. clean rooms). This is possible due to pure self-assembly nature of process, where the resulting structures are pre-programmed in their molecular and colloidal behavior. The properties of the materials thus prepared depend on tailored interactions between the molecular building blocks and substrate, which make this method highly flexible.

The common principle of NSL is quite simple (Fig. 3.1). Usually, colloidal nanoparticles are deposited on planar surface by self-assembling process mostly in the form of monolayer. The resulting ordered array of nanoparticles (colloidal mask) is used as template for various subsequent plasma etching and/or deposition processes. After selective plasma processing, the remaining colloidal mask is removed by means of lift off process which results in nanopatterned surface consisting of regular spots with different physico-chemical and/or topographical properties as those of original planar surface. Such surface can be further used for

selective immobilization of various biomolecules through covalent attachment to the exposed surface and preparation of the final nanostructured biointerface. There are several key parameters, whose variation influences the properties of resulting nanostructure. These include: (i) nanoparticles properties (material, size, charge); (ii) physico-chemical properties of planar surface; (iii) methodologies for mask self-assembling (drop casting, spincoating etc.); (iv) post-assembling modification of colloidal mask (e.g. plasma etching, selective patterning); (v) plasma processing and development of final nanostructured surface (etching, metal or polymer deposition etc). The main variations and their influence on NSL process are discussed further on.

### ***3.2.2 Preparation of colloidal mask***

A huge variety of submicron particles in colloidal suspensions can be used for preparation of lithographic colloidal mask, varying in type of material from which they are made, their dimensions and surface charge. Usually they have a spherical or quasi spherical shape with controllable dimensions within the nanometric range. Due to their frequent use in many application fields, they are readily available on commercial base. Colloids can be synthesized in a number of materials including polymers (e.g. block copolymers, dendrimers) [53-55], metals (e.g. gold, platinum, palladium), semiconductors (quantum dots) or metal-polymer nanocomposites [56-58]. Among the other, polystyrene (PS) nanoparticles are frequently employed for NSL [59-63] since they can be synthesized monodispersed and with a wide range of surface chemistries and charges. Although they are available with a diameter smaller than 100 nm, silica nanoparticles are mostly used in this dimension range due to their

lower size dispersion [60,64]. Selection of appropriate colloids is crucial for successful nanopattern generation, as well as surface charge and size of particles are critical criteria. Dispersion is also important factor since it influences the frequency of defects in the obtained array.

The colloidal mask is usually self-assembled on a planar base substrate which will be patterned. The physico-chemical properties of surface are tailored according to both the needs of the final application and the special requirements of lithographic process. Properties such as the wettability and the surface charge help the formation of ordered colloidal template because they influence the solvent evaporation process and the substrate-particles interactions. Conductive [59], insulating [52], optically transparent [47,52,65] or other types of materials can be used as base substrate. Most frequently, glass or silicon [59-61,64,66] covered with thin layers of metals [59,64], metal oxides [60] or with various types of polymers [64,66,67] have been exploited. Self-assembled, spin-coated or plasma polymerized thin films may be prepared on base substrate [63,68,69]. Since the final nanopattern is mostly obtained by plasma etching process, the etching rate of base substrate has to be equal or higher than colloidal mask, otherwise no pattern could be transferred.

**Colloidal nanoparticles** are dispersed on substrate in appropriate solution and are electrostatically self-assembled into 2D crystalline structures as the solvent evaporates. Driving forces of the assembly (i.e. electrostatic particle-particle and particle-substrate interactions, hydrodynamic interactions and diffusion) result in a hexagonally ordered nanostructure with the particles separated by an average distance (Fig. 3.1b). The space between particles can be adjusted by changing several conditions or particle/substrate properties, influencing the assembling forces. The

ionic strength of the colloidal solution has influence on the range of repulsive interparticle electrostatic interactions [70]. With decrease of salt concentration, the interparticle repulsion forces increase, resulting in longer particle distances and decreased saturation coverage [60]. Ionic strength of the colloidal solution is therefore a simple way to control the interparticle distance in the colloidal mask. Similarly, other factors like pH of the solution [71], particle and surface charges [71,72], and particle size [73] play an important role in self-assembling process and have to be controlled in order to obtain reproducible pattern.

There are several methods used to spread colloids onto the base substrate. Probably the most simple approach is drop-casting where the solution of particles is simply added drop-wise onto the base substrate. While the solvent evaporates, the colloids remain on the substrate surface. Since during the evaporation the capillary forces between the particles dominate during the evaporation, they can be arranged in different geometrical configurations in order to minimize the space and the free energy of the system. Therefore, the rate of the solvent evaporation controls the degree of order in the pattern [74,75]. Other methods of deposition are represented by sedimentation [76], electrodeposition [77] or spin-coating [78,79]. Due to the parallel nucleation events of self-assembling, most of these methods inevitably lead to imperfections in the assembled 2D structures. Normally, the obtained defect-free area is not larger than several square micrometers. Further on, variation of nanoparticles size (polydispersion) alters electrostatic repulsion between individual pairs of colloidal particles, thus introducing dislocations [75].

Recently, alternative form of colloidal lithography has been presented [60], where charged particles adsorb randomly onto oppositely charged surface. The randomness

of the initial process of adsorption causes uniformity of array over large surface area without any imperfections and dislocations. Additionally, dip-coating as sequential assembly process may be used for fabrication of perfect, defect free arrays over large area [64], mainly due to the well controlled drying-front (liquid meniscus) and other conditions such as particle concentration and ionic strength. Contrarily to previous methods, capillary forces are identified as the basis of the assembly process which does not require any specific chemistry on either the template or the particles. Therefore, this method is generic and allows a large choice of both support and particle materials.

### **3.2.3 Plasma modifications and lithography**

Following the primary process of ordered nanosphere layer formation, the obtained nanopatterns can be used without further modifications for biological investigations [80,81] or, more frequently, various post-assembling processes are performed (e.g. dry etching or coating) in order to modify the geometry of periodic 2D colloidal mask or to pattern the base substrate. As an example, reactive oxygen plasma treatment is frequently used to modify the polystyrene particle size [61,82]. The ordered pattern becomes more *open*, since the particle size decreases. By variation of plasma exposition time, different sieve-like structures can be prepared from the same template (Fig. 3.1 c-f). Apart from size, the shape of particles becomes slightly ellipsoidal, due to the unequal plasma abrasion [60]. These structures are characterized by larger interstitial area compared to original mask which may be

useful for preparation of circular nanospots, columns or wells with different chemical and topographical properties from those of the base substrate.

Lithographic processing, utilizing e.g. reactive ion etching (RIE), allows the production of modified colloidal-derived nanotopographies [42,60,83]. Here, the assembled colloidal monolayer serves as mask, and protects the underlying base substrate from etching, except the interstitial area between the individual particles. As a result, nanopillars with diameter of colloidal particle can be prepared by etching of base substrate [46,84-87]. The dimensions and pillar profile is determined by etch time, gas, pressure and mask integrity. Other geometric bodies formed on colloidal lithographic mask may be hemispherical protrusions [42,88], cups [89], nanowells [90-92] or rings [93-95].

Apart from RIE lithography, colloidal mask is often used for selective deposition of various materials, predominantly metals (silver, aluminum, nickel, etc). After lift-off procedure, when colloidal monolayer is removed, a metal masks reflecting the interstices of the close-packed colloids assembled in hexagonal or triangular lattice arrangements is manufactured. Besides metals, various polymers (e.g. plasma polymerized) can be overlaid on mask, leading to homogenous surface chemistry of patterned features after removing the template nanoparticles [45,62,83]. It allows further modifications of defined chemical patterns and decoration with other functional molecules, biomolecules (proteins, DNA) or nanoparticles [83,96]. A final step which follows exposure of mask to RIE, is performed in order to remove the colloidal mask. Mostly, wet chemical etching methods are employed where particles are removed due to the combined effects of chemical etch and a net repulsive

interaction between the particle and the surface. Short time sonication usually helps the dissolution of mask [97].

#### **3.2.4 *Combination of NSL and other lithographic approaches***

Despite many advantages that NSL itself provides, there are some limitations in terms of flexibility to produce different patterns (shape and size, spacing between features, addressability of individual units etc.). Therefore, hybrid approaches in fabrication, that combine self-assembly principle of NSL and conventional lithography, are actively conducted to address these issues [98]. Successful attempts are reported where photolithography [99,100] or electrostatic fields [101] are used to pattern regions of particles. Here, conventional lithography or other patterning techniques are commonly used for fabrication of micro(nano)structured base substrates where self-assembling of colloidal particles is directed to selected area having certain chemical or topographic properties. As an example, combination of colloidal particles self-assembling and interference lithography has been presented [64]. Poly(methyl methacrylate) (PMMA) layer spincoated on chromium (36 nm) or SiO<sub>2</sub> (100 nm) coated silicon wafers has been used for line/space and hole patterns fabrication with periods in the 40–100 nm range by grating-based interferometer. Gold (50 and 15 nm) and silica (50 nm) particles in aqueous suspensions were self-assembled on PMMA by dip-coating. The difference in wettability (hydrophobic–hydrophilic contrast) between the polymer lines and the underlying surface affected the selective assembly of the particles.

Due to the simple fabrication and the low cost, the combination between NSL and soft lithography can potentially bring many future applications. Recently, a novel method entitled microcontact particle stripping ( $\mu$ CPS) has been introduced [59]. It combines the use of an elastomeric stamp as a basic component of microcontact printing ( $\mu$ CP) with colloidal lithography. The simple procedure is based on contact between the elastomeric stamp and substrate modified by monolayer of pre-adsorbed polystyrene particles. Particles from contact regions are removed. The remaining colloidal particles unaffected in non-contact regions can be further used as a lithographic mask. This method has been successfully applied with particles in the size range of 50-500 nm whereas the spacing of the particles is a multiple of their diameters (from 1.5 to 4). Other methods which use microcontact printing ( $\mu$ CP) are based on patterning of self-assembled monolayers (SAMs), which further facilitate a selective deposition of colloidal particles on chemically patterned surface [102,103].

A promising direction, by which some limitations (e.g. configuration disorders, spacing of individual colloids) of classical NSL can be overcome, is the self-assembling of block copolymers instead of colloidal particles which has been used for fabrication of periodic arrays with sub-100nm features [104,105]. Block copolymer lithography is in fact a fast growing field with many interesting applications. Similarly as in NSL, the driving force for nanostructuring using these polymers is the self-assembling. Due to enormous flexibility in chain properties and its behavior, various nanopatterns may be prepared, which are normally inaccessible for NSL. In this chapter, we will show only a few interesting examples of the method. Readers who are interested in more details should follow one of the recent reviews in this field [106,107]. An advantage of amphiphilic diblock copolymers, such as polystyrene(x)-

*block-poly(2-vinylpyridine)(y)* ( $PS(x)-b-P2VP(y)$ ) is that, under a suitable conditions (e.g. solubilized in toluene), they form core-shell micellar structure which enables the selective dissolution of the metal precursor salts and after the chemical reduction step, generation of mono-dispersed metal particles. Block micelles of copolymers containing gold nanoparticles have been used for self-assembling on glass substrate [108]. After exposure to hydrogen plasma, gold particles remain on the substrate surface in hexagonal patterns, whereas the polymer has been removed. The spacing between individual gold particles is set-up by properties of diblock copolymer used. Similarly, combination of block copolymer and e-beam lithography has been used for fabrication of various periodic and non-periodic patterns of Au nanoparticles, separated by distances not normally obtained by pure self-assembly [109].

### ***3.2.5 Application of NSL for sensor biointerfaces***

#### ***3.2.5.1 Biointerfaces based on protein nanoarrays***

Application of colloidal lithography in the fabrication of nanostructured surfaces for biosensors and other related biointerfaces is still in its infancy, but several representative examples of applications indicate the possible directions of future developments. Apart from biosensor interfaces, colloidal-derived nanotopographies currently under investigation show great promise in control of cell growth and adhesion to surface, altering gene regulation or inflammatory response [43,46,110,111] which may bring new interesting properties of functional medical devices, e.g. implants or tissue engineered constructs [112]. Despite their importance,

these applications will not be reviewed in this chapter. The interested reader should follow recent reviews in the field [74].

A key achievement regarding the generation of sensor biointerfaces using colloidal lithography is the ability to selectively bind sensing biomolecules on patterned areas and to retain their natural active conformation and favorable orientation. Once the molecule is selectively immobilized in nanoarrayed substrate, it can be used in many detection strategies, most frequently optical and electrochemical, to detect the analyte of interest. Recently, several attempts have been performed to show this possibility. Chemically nano-patterned surfaces with biologically relevant end groups such as carboxylic groups and anti-fouling polyethylene glycol (PEO) functionalities have been prepared by the combination of NSL and plasma deposited functional polymeric layers [68]. Plasma enhanced chemical vapor deposition (PE-CVD) is a low pressure and temperature process which allows the creation of thin films on a large variety of substrates with selectable chemical functionality, stability, density and coverage of the deposited films. Here, thin and negatively charged (carboxylic groups) hydrophilic plasma polymerized acrylic acid (PAA) film has been deposited on solid support using a glow discharge created from acrylic acid vapor. After assembling of 2D colloidal mask pattern of negatively charged polystyrene beads (diameter 200-1000nm) by dip-coating method, oxygen plasma etching has been carried out resulting in creation of PAA nano-domes. Following the plasma deposition of the PEO-like coating (protein resistant layer) and mask dissolution in ultrasonic bath, bovine serum albumin (BSA) has been immobilized selectively on PAA layer using standard conjugation chemistry.

Similarly, a horse spleen ferritin nanopattern has been prepared by selective protein deposition on gold cylindrical disks (20nm high, 120mm in diameter) covered by SAM of hydrophobic thiols [113]. Pattern has been obtained by oxygen plasma etching of polystyrene particle mask assembled on silicon wafer and covered by thin layer of gold. Non-specific binding of ferritin on the exposed silicon surface has been protected by selective deposition of PLL-PEG (PLL backbone and PEG side chain) amphiphilic copolymer monolayer. Another investigation has described collagen adsorption on model substrate exhibiting controlled topography and surface chemistry [88]. Substrates were prepared by gold deposition onto silicon wafers (smooth substrate) and onto a support with nanoscale protrusions created by colloidal lithography (rough substrate) and by subsequent functionalization with CH<sub>3</sub> (hydrophobic) or OH (hydrophilic) groups. Based on their results, authors concluded that, while the adsorbed amount of collagen is only affected by the surface chemistry, the supramolecular organization is controlled both by surface chemistry and topography.

A simple approach of functional protein arrays production which is based on self-assembling of polymer templates and proteins has been recently shown [114,115]. To create arrays of protein nanostructures with defined spacing, monodisperse latex spheres has been coated with desired protein (BSA, protein A and G) and deposited on mica (0001) or gold (111) surface. After drying, latex particles are displaced to expose periodic arrays of immobilized proteins, which remain attached to the surface and maintain the order and periodicity of the latex scaffold. Morphology and diameter of protein nanostructures thus prepared are tunable by setting-up the protein-to-latex ratio and the diameter of latex spheres [114]. Similarly, lysozyme periodic

nanostructures have been prepared on silicon by NSL, retaining their full activity [115]. Another interesting approach based on self-assembling properties of diblock copolymers has been introduced [116]. It has been shown, that chemical heterogeneity of self-assembled hexagonal polystyrene-*b*-poly(vinylpyridine) (PS-PVP) diblock copolymer micelles on flat surfaces can be successfully exploited as template for protein self-assembling in specific polymer nanodomains, thus creating high density ordered protein array. The properties of array may be easily tuned by size of underlying diblock copolymer. In order to show the possible exploitation of such nanoarray in biosensor applications, various proteins has been thus immobilized and their activity screened [117]. By immobilizing e.g. horse radish peroxidase (HRP), mushroom tyrosinase, bovine immunoglobulin G and green fluorescent protein, authors found that immobilized proteins retain their catalytic activity over 3 month and that their binding behavior is not affected by surface immobilization on diblock copolymer template.

Despite the potentiality of the NSL or block copolymer lithography for protein arraying has been shown in several attempts, a little work has been done to screen the biological functionality of proteins in arrays thus prepared. As an example, adsorption of fibrinogen on a substrate with nanoscale pits and its ability to selectively bind unstimulated platelets has been investigated [118]. Colloidal lithography has been used to create high density of nanometre-sized pits (40 nm diameter, 10 nm depth) in continuous thin metallic film vapor-deposited over top of the electrodes of quartz crystal microbalance (QCM) sensors or on silicon wafers. The multidomain protein human fibrinogen was adsorbed on the structured and planar surface as control sample due to its similarity with pits size. The ability of fibrinogen molecules to

specifically bind to receptors in platelet membranes has been correlated to both nanoscale chemistry and surface topography. No specific binding of unstimulated platelets during the initial phase of interaction was observed on fibrinogen bound to flat surfaces with homogeneous surface chemistry. On the contrary, fibrinogen bound at topographically structured surfaces (both chemically homogeneous and chemically patterned surfaces) exhibited significant specific platelet binding. Authors speculate that the conformation or orientation of fibrinogen molecules is altered at surfaces which have nano-topography on the length scale of the individual molecules. The altered orientation/conformation on nano-structured surfaces may make binding sites available to the fibrinogen molecule, which can bind to membrane receptors on unstimulated platelets.

The assembly of single biomolecule arrays, where nanostructured surfaces are able to accept only one single biomolecule at individual binding site, with definable spacing and orientation and created on large sample area is interesting challenge since such surfaces may show molecularly defined environment for cell culture studies and optimal sensing properties in biosensors [119-121]. Recently, the preparation of such an array has been shown [108,121] using nanostructured gold dot patterns prepared by micellar diblock copolymer lithography already discussed in this chapter. Gold nanoclusters with defined diameter (approx. 6 nm) and lateral spacing of 30, 96 and 160 nm have been prepared on glass and the interstices between them have been modified with monomolecular film of mPEG-triethoxysilane in order to prevent non-specific binding of proteins. Afterwards, gold nanodots have been modified with short thiol-nitrilotriacetic (NTA) chelator molecule. Further on, recombinant proteins (Agrin, N-cadherin) having 6 Histidine (6 x His) tag have been immobilized on

oriented manner through specific NTA-His tag bound and their presence detected by primary and secondary fluorescence labeled antibodies, as well as by atomic force spectroscopy (AFM). As result, up to 70% of gold particles creating the nanopattern have been modified with only a single functional biomolecule at molecularly defined density and locations. Due to the generality of immobilization method, identical arrays can be prepared for every biomolecule available.

All these examples show, that nanotopography can significantly influence structure and functionality of adsorbed proteins, when correct dimensions and topography are established. Similarly as observed for immobilization of biomolecules on nanoparticles with smaller dimensions [122,123], it turns out that the smaller interaction area between the nanostructured surface and biomolecule can affect the secondary structure to smaller extent compared to planar surface. Therefore the natural activity and functionality of protein is retained to high degree. In ideal case, the nanostructured element has dimensions similar to dimensions of immobilized biomolecule [62,118,121].

#### *3.2.5.2 Biointerfaces for localized surface plasmon resonance biosensors*

One of the most interesting features of nanostructured layers of metals are their unusual optical properties, which can be used for fabrication of ultrasensitive surface plasmon based biosensors. Noble metal nanoparticles normally exhibit a strong UV-visible adsorption due to the resonance between the collective excitation of conduction electrons and incident photon frequency [47,48]. This phenomenon is known as **localized surface plasmon resonance (LSPR)**. Due to the extremely large molar extinction coefficients (about  $3 \times 10^{11} \text{ M}^{-1} \text{ cm}^{-1}$ ) [124,125], intense signals can

be obtained using spectroscopic methods, which predetermines their use as optical sensors and biosensors [47,48,126,127]. Based on theoretical model of Mie [128], the intensity of the LSPR spectrum depends on a number of parameters, such as nanoparticle radius, material, dielectric constant, and interparticle spacing [129,130]. A common effort in the field is to find synthetic routes of nanoparticle fabrication in order to tune and precisely control their plasmonic properties. The simplest and mostly used approach is based on reduction of metal salts in solution which results in colloidal suspension of metal nanoparticles. Highly sensitive, LSPR biosensors have been realized based on the change of absorption UV-VIS maxima upon interparticle coupling. Complementary DNA colorimetric sensing has been shown, where the change in color is observed when nanoparticles are brought together by the hybridization event [131-133]. The limits of detection (LOD) reach femtomoles of target oligonucleotide which is almost 100-fold lower than conventional fluorescence assay [131].

Despite its sensitivity and simple procedure, the main disadvantage of the solution-based LSPR nanoparticle biosensing is the non-specific, irreversible and difficult to quantify particle aggregation [48]. Therefore, surface confined nanoparticle arrays may be employed for biosensing purposes instead of colloidal suspensions, to easily overcome the most of the difficulties. NSL has been successfully used to structure surface-confined triangular silver nanoparticles by metal deposition over polystyrene nanosphere mask on glass substrate [47,48]. The silver nanodots (100 nm in plane and 51nm out-of-plane width) have been modified with SAM from mixture (3:1) of 1-octanethiol (1-OT) and 11-mercaptoundecanoic acid (MUA) and further with biotin through zero-length coupling agent on carboxylate groups. The maximum of

observed plasmon resonance ( $LSPR_{\lambda_{max}}$ ) increased (red shift) at each modification step: from 561nm up to 609 nm after final modification step. In order to simulate an antibody-antigen binding as one of the possible future application of such optical biosensor, the calibration curve for streptavidin [47] and anti-biotin [134] binding has been obtained as the function of red shift of  $LSPR_{\lambda_{max}}$ . The LOD calculated from response curve has been lower than 1 pM for streptavidin and 100 pM for anti-biotin with 27 nm and 38 nm of maximal plasmon peak shift for each case. It was also shown, that by changing the shape, size and material composition of metal layer is possible to tune the sensing capability of LSPR sensors [135,136]. By immobilization of mannose on silver triangles, the carbohydrate binding protein (concanavalin A) has been used for tracking the response sensitivity as the function of height of silver nanodots [137]. Results show that overall response of the nanosensor increases with decreasing nanoparticle height.

Apart from metal nanodots, nanoring structures represent high potential to surface plasmon sensing at nanometer scale. This is mainly due to their tunable plasmon resonances and large empty volume which provides more spaces for molecular attachment [95,138]. A low cost method of producing large area ordered metal nanoring arrays based on NSL has been presented [95]. Close-packed SAM of polystyrene monodisperse spheres were formed on silicon substrate by spin-coating method. A layer of gold was sputtered onto colloidal mask on vertical incidence sequentially followed by reducing the gold-capped polystyrene spheres from the topside by ion polishing. The inner diameters, wall thickness and wall height of gold nanorings have been tuned by the size of PS spheres, and by the process parameters

of RIE, sputtering and ion polishing. Such tuning of metal nanoring structures leads to fine and flexible controlling of plasmon resonances of the nanorings [95].

Recent efforts in optical device fabrication based on LSPR detection have stimulated the development of sensitive, simple and label free detection of wide range of analytes in medical diagnostics, environmental and chemical analysis. The key factor which influences its further development is the ability to precisely control and tune the parameters of optically active metal array. Although novel approaches have also emerged, NSL lithography belongs to one of the simplest methods, by which such surfaces can be efficiently prepared and studied. Therefore, its further development in this field can be envisioned.

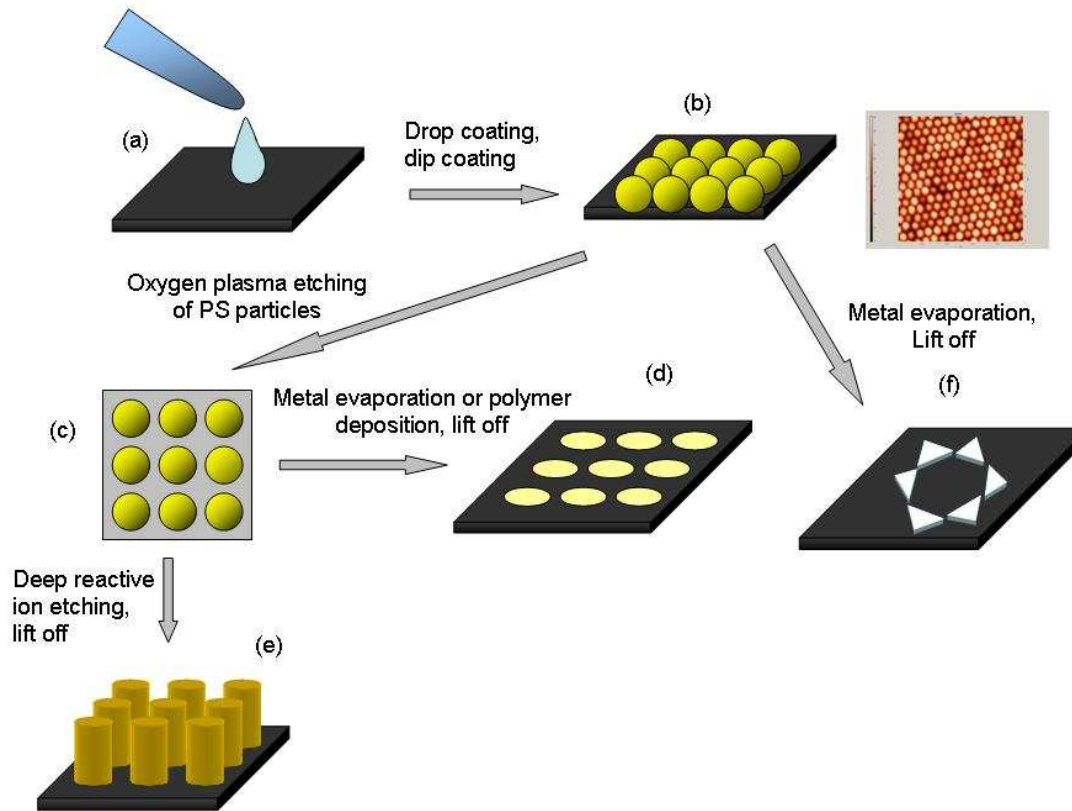


**Fig. 3.1- Basic principles of nanosphere lithography.** Solution of spherical nanoparticles is drop or dip coated on the flat base substrate surface (a); after evaporation of solvent, the hexagonal 2D array is spontaneously formed (b); on the right side: AFM image of 200 nm polystyrene monolayer; by oxygen plasma etching, the size of polystyrene particles can be decreased (c); metal or polymer maybe deposited in the interstitial area providing sieve-like structure after lift-off of polystyrene nanoparticles (d); by deep reactive ion etching nanopillars of the same material as base substrate can be prepared (e); metal nanoparticle triangles may be also prepared by metal evaporation over the structure (b) and subsequent lift-off (f).

### 3.3 Nanoelectrodes Ensemble for Biosensing Devices

#### 3.3.1 Electrochemical and electroless deposition of nanomaterials via templates

##### 3.3.1.1 Nanoporous membranes

The pores of filtration membranes represent a simple case of structural heterogeneity, whereby the discontinuity in the solid phase operates the selection for species with specific dimensional requirements. Deposition of nanomaterials can be carried out into the nanopores of ultrafiltration membranes with uniform, cylindrical or prismatic pores of particular size.

Nowadays, chemical sieves materials, such as glass matrices with nanostructured channels, zeolites, or nanoporous proteins, are worldwide available. Many research groups involved in synthetic routes by means of nanoporous templates make use of commercially available ultrafiltration membranes. Owing to the rather limited number of pore sizes and pore density of commercial products (e.g. from Anopore<sup>TM</sup>, Nuclepore<sup>TM</sup> or Synkera Technologies Inc.), other authors prefer to prepare their own templates in order to customize the geometric features.

A following chapter in the present book is dedicated to review the methods and the selected materials for nanopore fabrication. This part is specifically dedicated to applications of alumina and track-etched polymeric membranes as host templates for the synthesis of nanosized material.

Alumina membranes with regular pore distribution can be generally formed by electro-oxidation of aluminum substrates (high purity aluminum sheets) in acidic electrolytes using a two electrode cell. Cathode is generally made of aluminum, lead,

platinum or stainless steel [139-142]. The resulting structure of the porous oxide film consists of a uniform array of parallel alumina cells packed hexagonally, with a nearly cylindrical shape of the pores, high pore density and low diameter size distribution. The hexagonal self-order of the pores was justified by the presence of repulsive forces and the volumetric expansion associated with the anodization process [143-145]. By appropriate selection of the electrochemical process conditions, such as applied potential/current density, treatment time, concentration of the electrolyte mixture, temperature of the treatment, it has been possible to tune at will size and aspect ratio of the pores, preparing films with different thicknesses, pore densities and pore diameters from 5 to 1000 nm [144,146-152]. It was experimentally verified that:

- the thickness of the porous alumina increases linearly from 0.1  $\mu\text{m}$  to 10  $\mu\text{m}$  with the anodization time at a given voltage and temperature;
- the pore spacing varies regularly with the applied potential, typically in electrolytic solution of 25% sulphuric acid or phosphoric acid, or 15% sulphuric acid at fixed temperature;
- the pores density and the pores diameter are linearly correlated under controlled conditions [153].

According to some authors [154], in order to obtain high quality membranes, aluminum should be pre-treated in concentrated acid and plenty of distilled water to show a well polished, mirror-like surfaces. During the pores formation, aluminum is coated by a relatively thin non-porous insulating oxide layer, therefore the anode material surface is not directly exposed to the solution. Several strategies and procedures to separate the unoxidized foil from the porous oxide layer have been also

proposed. We leave the reader to peruse the literature [155-158] to follow the progressive efforts in improving the support quality.

Alternatively to brittle and rather rough alumina or silica membranes, nanoporous **polymeric membranes** prepared by the track-etch method can be used as templates of high flexibility and smoothness, often very stable in acids as well as in organic solvents and biologically inert. Such membranes can be produced with a relatively wide range of pore diameters. Polyethylene terephthalate (PET), polycarbonate (PC), polyimide (Kapton), polypropylene, polyvinylidene fluoride, and CR-39 (allyl diglycol carbonate) membranes were already used for this purpose [159]. PC, because of its high sensitivity to tracking and the mild conditions required for sensitization, is the foremost material used for preparing commercial track-etched membranes (Osmonics<sup>TM</sup> or Whatman<sup>TM</sup>), with pore diameters ranging from as small as 10 nm to as large as 10  $\mu\text{m}$  and pore densities between  $10^7$  and  $10^9$  pores  $\text{cm}^{-2}$ .

In order to prepare such templates, damage tracks in the polymer film are created with high energy particles (atoms or ions) and a treatment time which finally influence the number of the tracks and the resulting pores. Afterwards, the tracks are exposed to an alkaline etching solution, resulting in porous membranes whose dimensions strictly depend on both the etching time and the solution composition [160,161]. Depending on the etching conditions typical pores with symmetrical cylindrical or cigar-like shape can be generally produced. Under conditions of asymmetric etching, i.e. by treating one side of an ion-irradiated sample with an etchant, conical pores have been produced [162-164] on PC or PET membranes.

**Track-etched membranes** have a much lower pore density (of the order of  $10^9$  pores/ $\text{cm}^2$ ) than the alumina membranes ( $10^{11}$  pores/ $\text{cm}^2$ ), therefore the former are

more suitable as templates for producing low-density nanomaterials. The case of nanoelectrode ensembles will be discussed in the following sections as an example whereby a relatively low density is required. A limitation of track-etched membranes is strictly related to their production techniques that generate not uniform products. As a matter of fact, unless special and accurate procedures are accomplished, the resulting pores into PC membranes are not always parallel to each other, presenting an irregular shape and random spatial distribution.

#### 3.3.1.2 *Deposition of metals in porous templates*

Deposition of metals have been successfully attempted on alumina, silica and track-etched polymer membranes, according to different ways.

Electrochemical deposition of metals has accomplished into the pores of the membrane, just on the side which has been treated with a conductive layer (typically of 100-1000 nm) [165-182]. This approach is based on the assumption that template membranes are robust enough to tolerate hard treatments, such as plasma or vacuum deposition. In such experiments, the coated pre-sputtered thin layer is connected to a copper wire and set-up into an electrochemical cell, where the template membrane acts as the cathode and an external counter electrode as the anode. The deposition can be carried out both under galvanostatic or potentiostatic conditions. Literature data report gold electrodeposition into alumina, mica or PC templates in form of nanowires or nanorods [183-186], as well as deposition of silver, cobalt, nickel, copper, rhodium nanowires [187-189], iron nanotubes or cigar-shaped nanoparticles into polymers [168,190], palladium, platinum, tin nanoparticles or single crystal nanowires both into alumina and PC [191-193]. In the case of track-etched PC

membrane, it was verified that the addition to the plating solution of 1-2% gelatin generally improves the hydrophilic properties of the membrane with effective increase in the reproducibility of electrodeposition [166]. Metal sputtering was necessary to firstly create the conductive layer. The subsequent process is based on the progressive growth and filling of the pores, from the bottom metallic layer towards open ends of the pores, which normally results in solid rather than hollow nanostructures (i.e. formation of nanowires or fibers, not tubes) [153,194,195]. Alternatively to the deposition of single metal in form of continuous nanowires, segmented nanoparticles or composed multilayered nanofibers with different metals can be created as well. In the latter case, the growth of nanofibers consisting of the same metal of the conductive layer is in some way limited by the electrodeposition of a second metal. The original metal foundation is etched away in a following treatment, leaving the nanoparticles composed of the second metal into the pores of the template. Such a formation must be performed with a removable metal (for instance silver is attached by nitric acid) which acts as a foundation for the metal to be deposited in the second step [196,197].

The most experimented methods for the **electroless deposition** of metals in form of nanostructures involve the presence of chemical reducing agents to plate the material from a solution onto a surface. The low kinetics of the homogeneous electron transfer from the reducing agent to the metal requires a catalyst, which should be applied to the surface to be coated in order to accelerate the reaction rate. The thickness of the metal film deposited can be controlled by modulating the plating time. The principles of electroless deposition into templates have been exemplified in the case of gold deposition by Martin and coworkers for the fabrication of nanotubes or nanoelectrode

ensembles [25]: the specific case will be extensively described and discussed in the following sections.

Differently from the electrochemical procedure, the electroless methods with templates allow for the deposition of metal layer into the activated sites on the pore walls without requiring any conducting layer.

Nanomaterials tend to progressively grow from the pore walls towards the center of the cavity. For this reason, stopping the deposition at relatively short times, hollow metallic nanostructures can be generated into the template. In fact, it was experimentally observed that the production of gold nanotubes is realized decreasing as much as possible the size of the metal grains which constitutes the walls, for instance working at a pH condition of around 8.0 in the deposition bath [153].

After completion of the metal deposition, the template membranes can be used in the original form containing nanostructured metal or alternatively, they can be dissolved to leave arrays of nanowires/nanotubes attached at one end to a conductive electrode. In the former case, it is possible to obtain separation membranes with metallized nanopores that enable chemical functionalization of metal for different purposes: one of the most diffused examples in surface chemistry for biosensing applications is using the thiol chemistry [196,198]. As it will be shown in the following discussion, metal nanowires need to be deposited and kept inside the membrane, to obtain a continuous ensemble of nanoelectrodes.

If the resulting objects of the deposition are going to be free nanostructures in the form of nanowires, nanotubes or nanocones, their separation from the host membrane is required. Nanomaterials may be separated from track-etched template by dissolving the latter in a suitable organic solvent: PC membranes are soluble in dichloromethane,

PET in 1,1,1,3,3,3-hexafluoro-2-propanol. Alumina/ceramic membranes are shown to be soluble in strong alkali solution (such as KOH or NaOH), whereas polymers can be also etched by oxygen plasma treatment [25,153,168]. A criterion for the selection of the most suitable template may sometimes lie on the compatible matching between the metal to be deposited and the agent able to remove the membrane. Other *hybrid* deposition techniques including metals/composite into host templates are not further investigated in this chapter. It is the case of the chemical deposition of carbon/gold composite nanotubes in alumina templates by impregnation with a solution of diluted hydrogen tetrachloroaurate (HAuCl<sub>4</sub>) and acetone as reducing agent [197], as well as the intriguing synthesis of nanoparticle nanotubes inside the pore walls of silane-treated alumina, according to a self-assembly mechanism [199], or the formation of gold nanotubes by RF-sputtering of gold into nanoporous template [200].

### 3.3.1.3 *Characterization of nanomaterials in porous templates*

The characterization of such nano-structures can be done by several instrumental techniques including spectrophotometry (optical features are useful for defining the shape and spatial distribution of the nanostructures), voltammetry, optical microscopy, atomic force microscopy (AFM) and scanning (SEM) or transmission electronic microscopy (TEM).

SEM or TEM analyses (and to a less extent microthomy analyses) are typically used in morphological characterization of nanostructured materials obtained by template synthesis. The image resolution generally tends to improve as the nanomaterial is separated from the host membrane. In this case microscopic investigations have shown curious mushroom shapes, or *spaghetti* like metallic nanostructures after

removing the PC membrane with the suitable organic solvents [25,168,171]. TEM and high resolution TEM images of nanostructures were also obtained even without removal of the membrane, owing to the transparency of PC to electron-beams, although possible interactions between the beam and the polymer can generate distortions and artifacts [25,153,201].

### **3.3.2 Gold nanoelectrode ensembles**

The gold electrode has often been used as a transducer in electrochemical biosensors for several good reasons. One of the most intriguing characteristics, which is important in using functionalized surfaces for biosensing purposes, is the tendency to form self assembled monolayers or deposited multilayers through thio- or amino-coordinate derivatives.

Nanoelectrode ensembles (NEEs) fabricated by growing metal nanowires/fibres into the pores of a template, are nanotechnology tools which actually find application in a variety of fields ranging from electro-analysis to sensors and electronics. Here is described the synthesis of gold nanowires into PC membranes with controlled pore size using an electroless deposition method. The density of the template nanopores determines the number of nanodisks per total surface (pores  $\text{cm}^{-2}$ ) and correspondingly, the average distance between the nanowires, as the basic elements of NEEs.

Production of gold NEEs here described is based on the pioneering work of Martin's group [25], recently modified in order to optimize the resulting product and

to obtain a well defined nanostructure for the specific application. In brief, the electroless plating of gold NEEs consists of three main steps.

a) *sensitization* with  $\text{Sn}^{2+}$  solution: PC is firstly kept for 2 h in methanol, then immersed for 45 min in a solution of 0.026 M  $\text{SnCl}_2$  and 0.07 M trifluoro-acetic acid in equimolar mixture of methanol and water as the solvent; as previously reported, track-etched PC membranes are preferred for NEE fabrication over alumina membranes because of their smaller pore densities and their lower fragility.

b) reduction of  $\text{Ag}^+$  to produce discrete silver nanoparticles: after accurate rinsing with methanol, the sensitized membrane is immersed for 10 min in 0.029 M  $\text{Ag}[(\text{NH}_3)_2]\text{NO}_3$  at controlled pH.

c) galvanic displacement of silver particles and reduction of gold: the membrane is immersed into the gold plating bath which contains a commercial solution of  $7.9 \times 10^{-3}$  M  $\text{Na}_3\text{Au}(\text{SO}_3)_2$ , (e.g. Oromerse<sup>TM</sup> Part B, from Technics Inc.), 0.127 M  $\text{Na}_2\text{SO}_3$  and 0.625 M formaldehyde; after 15 h of electroless deposition additional 0.2 mL of formaldehyde are added to continue the deposition for further 9 h, after that the membrane is rinsed with water, immersed in 10%  $\text{HNO}_3$  to eliminate any surface traces of tin or silver, and dried in oven at 150°C to stabilize the resulted deposition. It was already observed that depending on the mechanism of growth of such nanostructures into the pores, at short plating times only gold nanotubes are formed, whereas the complete filling of the pores to accomplish gold nanowires requires 24 hours or more of electroless plating [25]. Another interesting observation is that the deposition velocity decreases when performing the overall process at a temperature between 0°C and 5°C. The original synthetic route was tested during the last years by varying the treatment time or the reagents concentration for the surface activation

both in  $\text{SnCl}_2$  solution and in ammoniacal  $\text{AgNO}_3$  for silver nanoparticles deposition. Basically, the key step of the synthetic procedure resulted the immersion of the membrane in gold plating solution. Gold nanotubes or nanocones [162,163,196,202] were also fabricated adopting a different treatment time under buffered controlled conditions (pH 10). From our practical experience, even  $\text{AuCl}_4^-$  as precursor can be used instead of the commercial solution of  $\text{Na}_3\text{Au}(\text{SO}_3)_2$ : after 24 h of immersion at  $4^\circ\text{C}$ , gold NEEs into the nanopores of track-etched PC membrane (nominal pore size 30 nm, thickness 10  $\mu\text{m}$ , pore density  $6 \times 10^8$  pores  $\text{cm}^{-2}$ ) were successfully created. Both the front and rear side of the membrane are coated with a thin gold layer.

#### 3.3.2.1 Morphological features of **gold nanoelectrode ensembles**

SEM observations, as the one reported in Fig. 3.2, show the successful formation of gold nanowires into PC membranes with a narrow size distribution and a mean diameter of 30 nm, adopting the synthetic method above described. A SEM model JEOL JSM-5510 was used for the characterization of nanowires reported in Fig. 3.2. The microscope is equipped with an Oxford Instrument EDS 2000 microanalysis detector and software for the elementary analysis. No sample coating was required for SEM observations. The image was obtained after peeling away the metal layer grown over the front side of the template membrane. Nanodisks emerging from the template are clearly visible from the figure with the typical fading lines behind them representing traces of the nanofibers that grew inside the membrane. The observation of such traces is possible because of two main reasons: firstly, the PC membrane is partially transparent to the electron beam; secondly, the nanofibers are not perfectly aligned parallel to the surface, as a consequence of the membrane production

procedure [25,153,166]. The density of deposited nanowires can be approximately calculated from a sample microscopy image, taking into account a defined area of investigation. For instance, since an area of  $9 \mu\text{m}^2$  is considered in Fig. 3.2, a nanowire density of around 6 pores  $\mu\text{m}^{-2}$  has been inferred. Such value is perfectly in accordance with the declared pore density of commercial membrane, confirming the process of pores filling with gold had been successfully accomplished. NEE can be either used as platform for immobilization of biomolecules (i.e. still including the nanostructures into the host membrane) or as free standing assembly of very small ultra-microelectrodes confined in a rather small space. In the former configuration higher mechanical stability is accomplished, owing to the presence of the membrane, hence this is the preferred configuration for biosensing purposes. On the contrary, after the membrane dissolution, a simultaneous process of nanowires/fibers self-aggregation and folding down takes place, with a possible partial loss of their electrochemical properties. Fig. 3.3 shows two SEM images at different magnifications of gold nanostructures (mean diameter size of 50 nm) after dissolution of the template membranes with dichloromethane. Bundles of nanowires or disordered nanosized structures are still visible on the treated surface instead of free standing aligned gold nanofibers.

### 3.3.2.2 *Electrochemical features of gold **nanoelectrode ensemble***

An accurate description of the electro-analytical and kinetic behavior of NEE is beyond the scope of this chapter, but ref. 153 represents an updated and complete treatment of such objects, including: the evaluation of the main geometrical parameters involved, their relationships with current responses, and the corresponding

electro-analytical equations. As far as the present book is concerned, the general concepts with respect to the behaviour of NEE will be briefly recalled.

NEE can exhibit three distinct voltammetric response regimes, depending on the scan rate and reciprocal distance between the nanoelectrode elements, which is a function of the pore density of the template. Total overlap regime occurs when radial diffusion boundary layers of each single nanodisk overlap totally (small distance between nanoelectrodes); pure radial regime occurs when the nanoelectrodes behave independently (higher scan rates, larger distances between nanoelectrodes) and linear regime when the nanoelectrodes behave as isolated planar electrodes [25]. It was demonstrated that for electro-analytical applications the total overlap regime is the most advantageous one because of the higher faradaic-to-capacitive current ratio [153,204,207], which was calculated to be higher than the ratio in the case of conventional electrodes (CGE) with comparable geometrical area. This concept is reported in the following equation:

$$(I_F/I_C)_{NEE} = 10^2 \div 10^3 (I_F/I_C)_{CGE} \quad (3.1)$$

where  $I_F$  is the faradaic,  $I_C$  the double layer charging current. The numerator of both the ratios can be calculated from the Randles-Sevcik equation as here reported:

$$I_F = 2.69 \cdot 10^5 \cdot n^{3/2} \cdot A_{geom} \cdot D^{1/2} \cdot C_b \cdot v^{1/2} \quad (3.2)$$

where  $n$  is the number of electrons involved in the process,  $A_{geom}$  is the geometric area of the ensemble,  $D$  the diffusion coefficient,  $C_b$  the bulk concentration of redox

substance, and  $v$  the scan rate of the voltammetric cycle. The denominators for nanostructured and conventional electrodes depend, respectively, on the active and on the geometric area of the ensemble. Indicating the ratio between active and geometric area as in the following equation [207]:

$$f=A_{\text{act}}/A_{\text{geom}} \quad (3.3)$$

the application of Randles-Sevcik equation on both the systems results in a coefficient  $f$  spanning from  $10^{-3}$  to  $10^{-2}$ , which means that for NEEs detection limits are at least 2 order of magnitude lower than those of regular electrodes. The  $I_F/I_C$  ratios or, alternatively, the coefficient  $f$ , are useful to discriminate the good NEEs for electrochemical biosensing applications from the bad ones [205,207,209].

In our laboratory, **total overlap diffusion** regime was observed at gold NEEs fabricated from commercial PC track-etched membranes of 30 and 50 nm pores diameter. The large number of NEEs which were prepared according to the electroless procedure were selected on the basis of the electro-analytical response and the agreement between theoretical and experimental values [153]. For this purpose, a reversible redox probe with a known diffusion coefficient must be studied at defined experimental conditions (e.g. measuring the current peaks in CV at fixed scan rate and potential step). The theoretical ratio,  $(I_F/I_C)_{\text{theor}}$ , depending on well defined equations was compared with the experimental one,  $(I_F/I_C)_{\text{exp}}$ . Values must be in accordance with a tolerance of 5%.

As a redox substance  $\alpha$ -(ferrocenylmethyl)trimethylammonium cation was selected, analogously with previous works [153,204,207], because of its well known

behavior. Cyclic voltammograms in  $10^{-2}$  M  $\text{NaNO}_3$  as supporting electrolyte alone and in  $10\mu\text{M}$  of redox probe were recorded. It was calculated that NEEs satisfying the above criteria are not more than 50% of the overall NEEs prepared in laboratory.

The reachable potential window for gold NEEs was previously studied [25,206] both in the negative limit, which is influenced by the hydrogen evolution reaction and therefore depends on the solution pH, and in positive potential range which is given by the formation of gold oxide. The NEEs used at low analyte concentrations (typically from  $10\mu\text{M}$  to lower than  $1\text{ nM}$ ) gave faradaic peak current down to a few pA. By operating with suitable electronic amplification levels, at pH around 7 and micromolar analyte concentrations, a potential window of gold NEEs between  $-750$  and  $+800\text{ mV}$  vs. Ag/AgCl reference electrode (RE) was found [153]. Such a wide electro-activity range as well as the high sensitivities of NEEs to electron transfer kinetics are interesting characteristics that are being exploited in highly sensitive analytical techniques, such as in trace metals determinations and the observation of species with perfectly reversible and fast electrochemical behavior. To the best of our present knowledge, the electrochemical features of the metal nanomaterials, excepting gold grown in nanoporous templates, have not been so deeply investigated. In addition to applications for trace electro-analysis with well known reversible redox probes, such as ferrocene derivatives or ruthenium complexes, NEEs were used in CV at micromolar concentration levels of more complex redox systems such as organic mediators or methylviologen or heme-protein cytochrome c [204,206,207].

### 3.3.2.3 *Deposition of nanoelectrode ensembles on substrates*

So far, a limited amount of publications report the attempt to assemble NEE in handy electrodes for use in electrochemical cell or in flow injection analysis (FIA) systems. The early assembly based on gold nanoelectrodes consisted of a copper tape which was directly attached to the upper gold layer, acting as electrical connections. After insulating this multilayers configuration, a hole was punched into the upper piece of insulating tape to define a geometric area,  $A_{\text{geom}}$ , of  $7.0 \text{ mm}^2$  [25,204,207]. Recently partial modifications have been carried out to improve the electrical connection between copper and NEE: the copper tape was attached on the lower layer that completely covers the rear side of the host membrane. The upper gold layer was peeled away from the membrane and therein an insulator with a  $7.0 \text{ mm}^2$  hole was attached [204,208,209].

In our laboratories, gold nanowires have been coupled with carbon **screen printed electrode** (SPE) to give a novel, rapid tool for disposable biosensors, which has been defined as **nanoelectrode ensemble** on **screen printed substrate** (NEE/SPS). The NEE/SPS preparation is aimed to combine the advantage of the electro-analytical sensitivities deriving from the nanosized properties with the feasibility and versatility of screen printing technology in fabrication of easy to be used sensors [210-212].

For the preparation of SPEs, conducting and insulating inks were printed on polyvinyl-chloride substrate using a HT10 Fleischle<sup>TM</sup> screen printing machine [198,212]. Silver and carbon-graphite pastes for the conducting paths and the working electrode (WE), Ag/AgCl for reference electrode (RE) as well as dielectric pastes were purchased from GWENT Electronics Materials Ltd<sup>TM</sup> (<http://www.g-e-m.com>).

In order to assemble gold nanoelectrodes containing membranes with screen printed substrates, the upper gold layer was firstly peeled away from the front side of NEE

membrane, leaving exposed the gold nanodisks on the surface. The rear side has been soaked into a wet graphite ink pad, then the inked membrane has been gently deposited onto the graphite WE of a plastic homemade screen printed substrate [198]. As commonly used in **screen printing** procedures, the device has been accomplished by printing both the insulator and the RE layer. Fig. 3.4 shows the above described novel screen printing sequence for the production of disposable NEE/SPS. In each case, an active WE area of  $2.5 \text{ mm}^2$  is defined by the insulator geometry. Also NEE/SPS were tested with  $\alpha$ -(ferrocenylmethyl)trimethylammonium cation by CV at different scan rates and different concentrations. Typical voltammetric patterns of such redox tracer on NEE/SPS recorded at  $100 \text{ mV s}^{-1}$  showed a quasi-reversible behavior with an anodic peak ( $I_p$ ) at  $150 \pm 10 \text{ mV}$  and a cathodic peak at  $-20 \pm 1 \text{ mV}$  [198]. According to the characteristic of nanoelectrodes under total overlap diffusional regime, peak currents of the redox probe were 2 orders of magnitude higher than in the case of conventional macro-electrodes.

### **3.3.3 Nanoelectrode ensemble for **enzyme based biosensors****

#### *3.3.3.1 State of the art*

Selective, sensitive and accurate quantification of a specific analyte or group of analytes is the key requirement in many areas of analytical and bioanalytical chemistry, such as for clinical, agricultural and environmental analysis, as well as in food and beverage industries. In order to be used as reliable analytical tool, complementarily with traditional chemical methodologies (such as colorimetric, spectroscopic, chromatographic or hyphenated methods), biosensors must provide

high performances with good accuracy, precision, and long term stability for simple, rapid *online* or *in-situ* measurements.

The very promising feature of gold nanoelectrodes applied for electrochemical biosensors is their enhanced current sensitivity, as described in the previous sections and expressed in Eq. (3.1). The **sensitivity ratio** between NEEs and conventional macro-electrodes with comparable geometric area and materials has been already indicated as the discriminating parameter in the selection of nanostructures for biosensing applications. This might result in a lowering of the detection limit during the bioanalytical monitoring of some specific analyte.

On the other hand, as it will be shown in the following discussion of results, this advantage arising from the nanoparticles properties is not always maintained when biochemical immobilization is performed on the electrochemical probe. The complexity of structures such as proteins, cells or biomimic compounds, and the multiple layers accumulated on the original surface are the reasons that limit the resulting performance of electrochemical biosensors based on such nanoparticles.

NEEs were already used as working probe on copper, glassy or carbon-glassy electrode for the detection of different substances. The model system which has been used for preliminary investigation in a reliable electrochemical biosensing device was the enzyme glucose oxidase (GOx), whose structure and biochemical properties are well known.

In a recent work, gold NEEs were treated with UV-ozone and ethanol to remove any oxide deposit before the monolayer assembly, then the surface was treated with thiols to form a SAM, and successively with coupling agents for the enzymatic immobilization. After treatment with 3-mercaptopropionic acid and 2-

mercaptoethylamine as thiol compounds, the functionalized surface was respectively immersed in glutaraldehyde (GA) in phosphate buffer solution (PBS) and a mixture of imides at pH 3.5 [213]. Two different flow detectors with commercial glassy carbon WE were utilized for the amperometric detection of  $\beta$ -glucose, respectively with injection loop of 100  $\mu$ l and 20  $\mu$ l. After the optimization of the electrochemical and flow parameters, the authors compared the amperometric FIA response in terms of sensitivity, reproducibility and stability for both GOx based biosensors, distinguishing between the two different covalent immobilization of the enzyme (i.e. using glutaraldehyde and succinimide as coupling systems). A linear dependence of glucose on the signal in the analytical concentration range 0.2-30 mM was detected, even in presence of interfering substances [214].

#### 3.3.3.2 *Nanoelectrode ensemble on screen printed based biosensors*

Our contribution in the development of biosensors based on nanoscale material relies on the combination between screen printed substrates and gold NEEs, resulting in the so-called NEE/SPS biosensing devices, as previously reported and illustrated in Fig. 3.4. The aim of this preliminary work was to evaluate the specific response to a target substrate after immobilization of the corresponding enzyme on NEE/SPS. GOx (from *Aspergillus niger*, specific activity of 198 units per mg of solid) was again used as a biochemical model system to test feasibility of the sensing probe. NEE/SPS-based biosensors were tested under FIA conditions, their analytical performances were evaluated and compared to unmodified carbon or conventional gold electrodes on which GOx is immobilized at fixed concentration.

For this purpose a home made flow cell was used for the characterization of NEE/SPS and successively, for the amperometric detection of glucose with a GOx based biosensor. The microcell was depicted and described in our previous work [198] and was provided with peristaltic pump (Gilson™ Minipuls 3) to propel solution along a flow injection system, with a 115  $\mu$ L sample loop injection valve and volume (Omnifit™, Cambridge, England). All reagents, supporting electrolyte solutions, buffer carriers, were prepared from deionized water (Synergy 185 apparatus from Millipore™). All the other chemicals and solvents of analytical grade were used without further purification. Voltammetric and amperometric measurements, performed respectively under batch and FIA conditions, were conducted with the Autolab™ potentiostat PGSTAT10. Two experimented methodologies [198] were chosen for immobilization of GOx on gold element that can be simplified as in the following:

*a) Covalent immobilization of protein*

In the former device the sequence is based on three main steps (Fig. 3.5). Firstly, 3-amino-mercaptopropionic acid, also called cysteamine (CYS), was assembled on gold nanodisks either electrochemically (20 s of 21 mM CYS growth at +800 mV vs. internal RE) or chemically (after immersing for 16 hours the NEE/SPS in a solution of 21 mM CYS). The electrochemical deposition of CYS has already been demonstrated to be much faster and more effective on pure gold electrode than on other materials, resulting in electrochemically deposited multilayers (EDM) [215] on whose upper surface are available terminal amino-groups (-NH<sub>2</sub>). For this reason GA (12.5 % v/v, 1 hour of immersion) was chosen as the coupling agent in the second

step, followed by an accurate buffer washing to remove the excess of GA. Finally buffered GOx solution ( $6 \text{ mg mL}^{-1}$ ) was dropped on the activated surface and left to dry allowing for the formation of a covalent bond between the primary amine groups of the enzyme and the carbonyl group of GA. The resulting sensor was washed and stored overnight at  $4^{\circ}\text{C}$  before being assayed. This sensor configuration will be defined in the following discussion as GOx/EDM/NEE/SPS.

b) *Parallel immobilization of protein and deposition of conductive polymer*

In this device a spatial patterning of the enzyme on PC membrane with conductive wires on gold nanoelectrodes has been carried out. In this way, a direct electron transfer from the red-ox site of the enzyme to the electrode along the conductive polymer multilayer will be accomplished. As depicted in the sequence of Fig. 3.6, firstly, conducting cables of polyaniline (PANI) were electrochemically deposited by cyclic voltammetry from  $-0.4$  to  $+1.0$  V, using as a precursor  $50 \text{ mM}$  aniline solution in diluted sulphuric acid ( $0,5\text{M}$ ) [198]. The growth of PANI wires can be realized onto the gold nanostructures after few cycles, analogously as demonstrated on golden macroelectrode and other surfaces [216-218]. The active surface was immersed in a solution of  $10\%$  v/v aminopropyl triethoxy-silane (APTES), in order to obtain a terminal amino group onto the part of the membrane which is not gold-covered, then accurately washed with PBS (pH 6.8). The resulting surface was treated with GA ( $12.5 \%$  v/v) and again washed with PBS to remove the unbound GA. At this step free carbonyl groups facing the PC surface are ready to react with the terminal amino groups of the enzyme. Freshly prepared GOx buffered solution ( $6 \text{ mg mL}^{-1}$ ) was dropped on the activated surface and left to be covalently bound. This sensor configuration will be defined in the following as GOx/PANI/NEE/SPS [198].

The effectiveness of the electro-deposition of multilayers of CYS was proven by the cyclic voltammograms and the corresponding oxidation peaks centered at approx. +800 mV vs. internal Ag/AgCl RE that decreases after a few scans in the case of both gold SPEs [215] and gold NEE/SPS [198]. Chrono-amperometry current response corresponding to the oxidation of CYS on the surface has been therefore performed at +800 mV vs. internal Ag/AgCl pseudo-reference electrode (RE). As shown in Table 1, the average peak for CYS grown on NEE/SPS is compared with CYS deposited on gold screen printed probes, applying the oxidation potential of +800mV vs. platinum RE in a two electrode configuration. Current signal for CYS deposited on NEE/SPS is of two orders of magnitude lower than in the case of gold macroelectrodes obtained by galvanic deposition (column *a* of Tab. 1). On the other hand, considering the active area, taking into account the gold nanodisks density and the area of a single nanodisk, calculations of current density show higher values for nanostructured assembly (column *e* of Tab. 1 wherein current density is expressed in mA cm<sup>-2</sup>). Two different diameters of single nanoelectrode depending on the pore diameter size of the host template have been considered in such evaluation.

### 3.3.3.3 Analytical performance of NEE/SPS based biosensors

In both sensor configurations the flow injection conditions above described were experimentally optimized for the highest current signal. The working flow rate (0.4 mL min<sup>-1</sup>) and buffer pH (6.8) were fixed in both cases, by using the homemade flow-through detection cell and 115  $\mu$ L sample loop injection valve.

Unmodified NEE/SPS did not respond to glucose, confirming that aspecific oxidation of the substrate/analyte at the gold surface did not occur. Since the best

signal to noise ratio was achieved within the range +550/650 mV [198], an applied potential value of +600 mV vs. RE was chosen for such sensors in all the subsequent experiments.

In Table 2 the analytical performances of our sensor configurations (both GOx/EDM/NEE/SPS and PANI/GOx/NEE/SPS) are summarized while comparing such performances with those of an available reliable biosensing device for glucose detection [214] based on gold NEE (in Tab. 2 renamed as GOx/GA/MPE/NEE). An analogue comparison has been made under flow conditions with a biosensor for glucose based on commercial ceramic printed electrode (BVT Technologies<sup>TM</sup>, Czech republic), adopting one of the same immobilization procedure of GOx on golden working probe (herein indicated as GOx/CYS/Au SPE).

The linearity of response were found to be respectively for GOx/EDM/NEE/SPS  $1.0 \times 10^{-4}$  M to  $3.1 \times 10^{-2}$  M ( $R^2=0.993$ ) and for PANI/GOx/NEE/SPS  $1.0 \times 10^{-4}$  M to  $2.0 \times 10^{-2}$  M ( $R^2=0.998$ ). It is interesting to observe that the lower limits are always within the analytical range for glucose monitoring in blood sample.

At higher glucose concentration values, most probably saturation of enzymatic active sites takes place. The linearity can be estimated by using the Michaelis Menten equation with non-linear curve fitting: an apparent constant of 14.9 mM and 6.9 mM were respectively obtained for GOx/EDM/NEE/SPS and PANI/GOx/NEE/SPS: as expected these values are significantly lower than that of the native enzyme [219].

Sensitivity (the slope of the calibration curve) and LOD by Zund Meier method [220] as well as operational and shelf stability were all reported on Table 2 according to the recommended international definitions [221,222]. The achieved long term stability in FIA conditions for PANI/GOx/NEE/SPS biosensor suggests that chemical

covalent immobilization of enzyme on the surface took place. This observation is an encouraging result to assess the specific reaction between the silane-derivative compound and PC and consequently, the selective addressable immobilization of proteins only onto the polymer part of the membrane.

The amperometric FIA responses were also compared for both sensors at the concentration level of 0.5 mM glucose. The plots have been normalized in terms of the current peak height for both sensor configurations; the PANI/GOx/NEE/SPS sensor showed a faster response which depends on a more effective charge transfer to the electrode along the PANI wires (graph reported in ref. 198). In each case, when using PANI wires with covalent immobilization of GOx, it was achieved an improvement of performance, in terms of the linear dynamic range, reproducibility (4.4% of relative standard deviations) and LOD.

Finally, it is worth to note that a comparison between the features of bare NEE or NEE/SPS (usually selected by their performances operating in CV) and those of the enzyme based NEE or NEE/SPS biosensors under amperometric flow measurements are meaningless. As already mentioned in previous sections, the effect of nanostructured surface properties in term of high signal to background ratio require further investigations whenever the same nanosized component is implemented in a more complex configuration, such as a biosensing devices. The combination of diffusion pathways at the NEE and flow lines under the constrained geometry of a thin layer flow detection cell should be envisaged as well.

### 3.3.4 Concluding remarks

The integration between nanotechnology and electrochemical biosensors have found a remarkable example in the NEEs enzymatic based biosensor, where nanoelectrode ensembles synthesized by templates are deposited on several supports. Implementation of a novel disposable device based on nanoelectrode ensemble on screen printed substrate has been shown. In this way, the well-known advantages of nanostructured material properties (i.e. the high sensitivity) have been coupled with the typical features of thick film technology in screen printing production (such as disposability, flexibility, durability of the product under flow injection conditions). The electroanalytical properties of NEEs were extensively studied in previous works and were considered as the basis for the realization of NEE/SPS based biosensors. Exploitation of nanosized surface to enlarge the range of such possibilities is discussed, especially for the enhanced signal-to-background ratio of the gold nanoelectrode assembly (from two to three order of magnitude higher than conventional macroelectrode with comparable geometric area).

Immobilization techniques of model protein (for instance glucose oxidase) have been presented in association with the formation of self assembled monolayers and electrochemical deposited multilayers. The concept of reversible, oriented and addressable immobilization of special proteins on specific parts of the active sensing surface has been also recalled.

Simple enzyme immobilization on gold NEE and NEE/SPS by means of commonly used coupling agents or, more specifically, parallel immobilization of enzyme on the polymeric part of the membrane and polyelectrolyte on gold nanostructures have been

performed. The latter solution has been introduced to be extended in some application for third generation biosensor, wherein a mediatorless detection is required, thanks to the possibility to achieve a direct electron transfer between red-ox proteins and modified gold nanoelectrodes through the conducting polymer cables. A model protein was used to show the feasibility of such approach to activate the surface with specific biomolecule for the detection of an analyte or a class of analytes in many electrochemical biosensing applications, such as food or beverage industries, environmental, and clinical analyses.

Furthermore, the perspective of efficient parallel immobilizations, respectively on metal area and polymeric part opens up the way to multifunctional electrochemical devices with different customized sensitive elements in different points of the same sensor. Multiparametric electrochemical detection for simultaneous analysis at low costs may be designed insofar successful and reliable scientific results will be accompanied by the industrial scale-up of such devices.

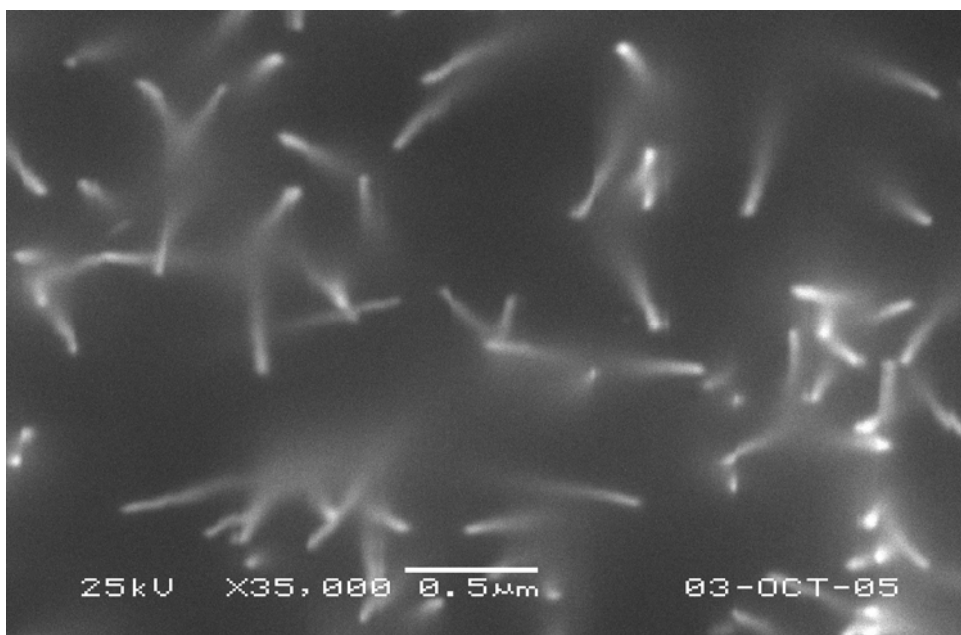


**Figure 3.2-** SEM image of gold nanoelectrode ensemble grown into polycarbonate nanoporous membrane (from Unipore™), according to the electroless procedure; nominal pores size: 30 nm, pores density:  $6 \cdot 10^8$  pores  $\text{cm}^{-2}$ ; scanning electron microscope was JEOL JSM-5510 Low Vacuum model.

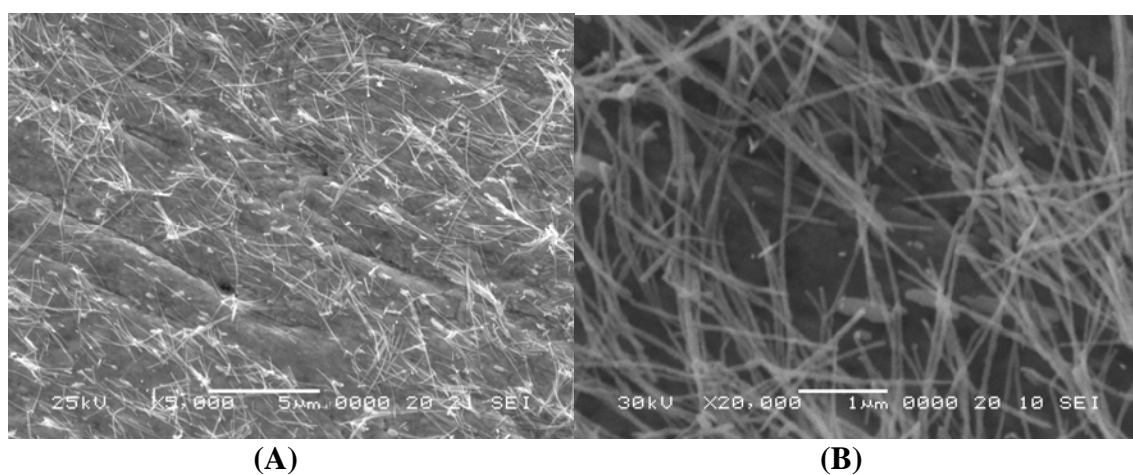


**Figure 3.3-** SEM image of gold nanoelectrode ensemble by electroless synthesis after dissolution of the polycarbonate template membrane (from Unipore<sup>TM</sup>) with dichloromethane. Images taken at two different magnifications; A) energy beam: 25 kV, scale bar: 5  $\mu\text{m}$ , magnification:  $5 \times 10^4$ ; B) energy beam: 30 kV, scale bar: 1  $\mu\text{m}$ , magnification:  $2 \times 10^5$ . Scanning electron microscope was JEOL JSM-5510 Low Vacuum model.

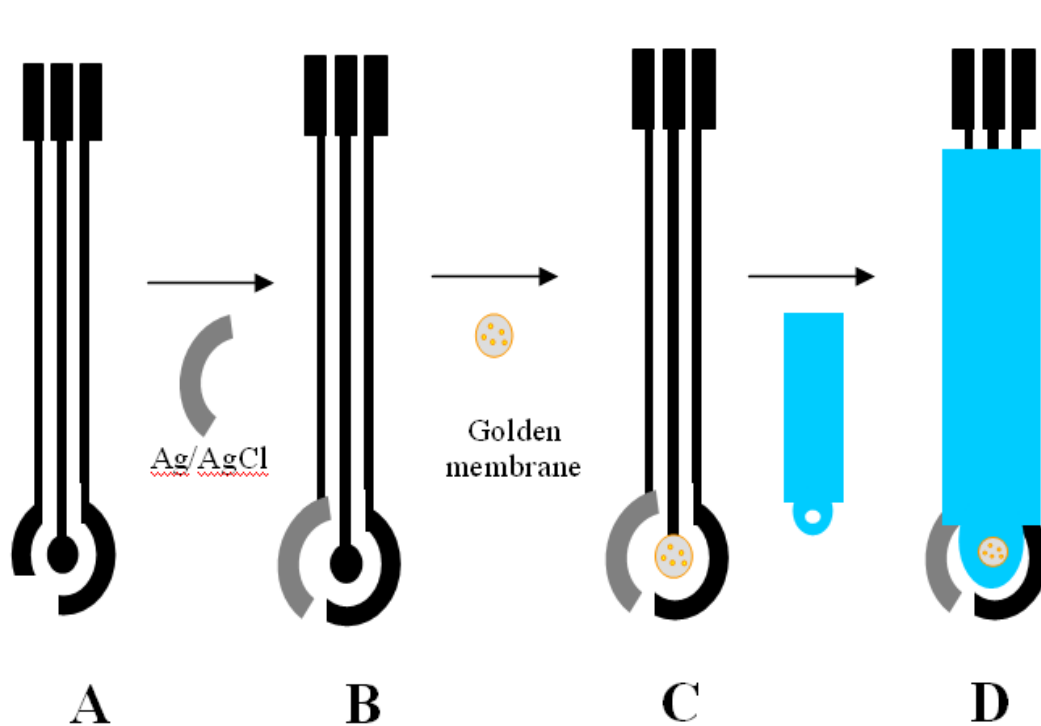


**Figure 3.4-** Schematic sequence of the NEE/SPS preparation [198]; A) carbon graphite tracks and contact pads by screen printing; B) Ag/AgCl paste deposition for reference electrode; C) deposition on the working of the NEE based membrane; D) dielectric paste screen printing.

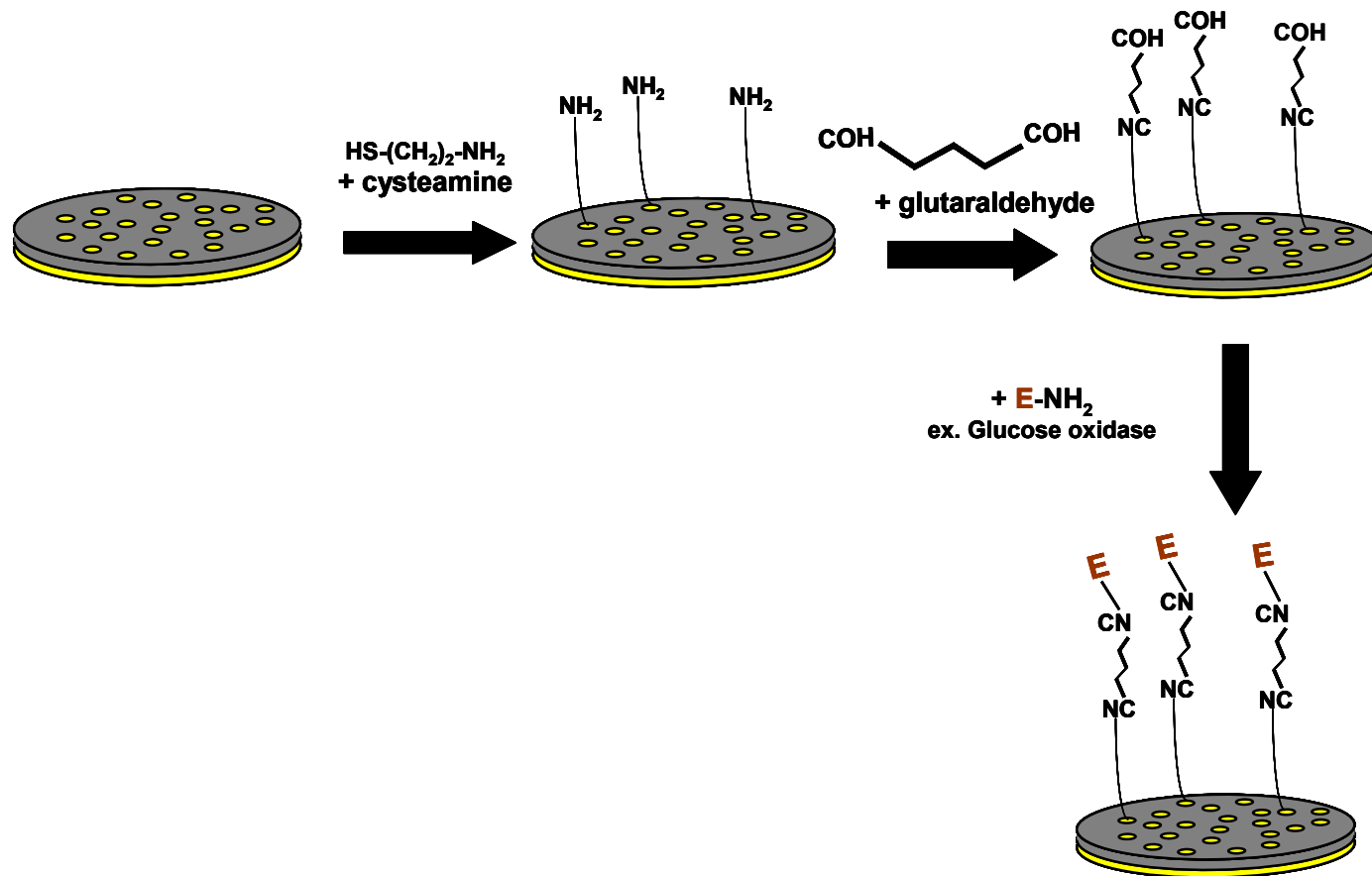


**Figure 3.5-** Schematic representation of the covalent enzymatic immobilization via cysteamine (3-amino mercatopropionic acid) and glutaraldehyde on gold nanoelectrodes ensemble/screen printed substrates; distance of gold nanodisks and dimensions of the objects are not in scale.

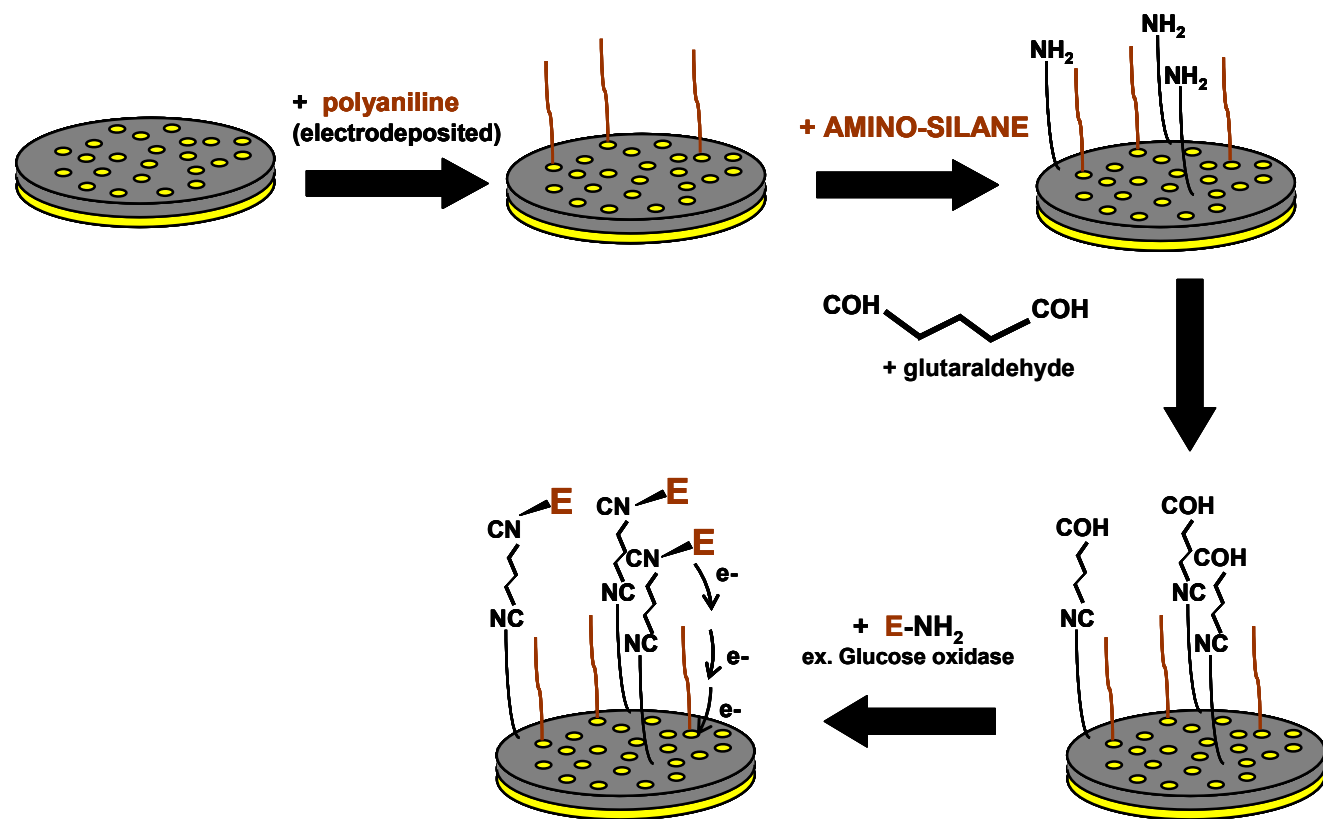


**Figure 3.6-** Schematic representation of the enzymatic immobilization (via aminopropyl triethoxysilane/glutaraldehyde) on polycarbonate membrane with parallel electrodeposition of conductive polyaniline (red wires) on gold nanoelectrodes; distance and dimensions of the objects not in scale.

	(a)	(b)	(c)	(d=bx c)	(e=a/d)
Electrode Probe	Peak current Ip ( $\mu\text{A}$ )	Geometric area ( $\text{cm}^2$ )	Conversion Factor *	Active area ( $\text{cm}^2$ )	Current density ( $\text{mA cm}^{-2}$ )
<b>Au</b>	625.0	0.143	*1.1330	$1620.00 \cdot 10^{-4}$	3.86
<b>Au NEE</b> [25,204,209]					
pore diameter=30 nm	0.5	0.071	**0.0042	$3.07 \cdot 10^{-4}$	<b>1.66</b>
pore diameter=50 nm	0.5	0.071	**0.0118	$5.95 \cdot 10^{-4}$	0.60
<b>Au NEE/SPS</b> [198].					
pore diameter=30nm	1.5	0.025	**0.0042	$1.08 \cdot 10^{-4}$	<b>14.15</b>
pore diameter=50 nm	1.5	0.025	**0.0118	$2.10 \cdot 10^{-4}$	5.09

\* dimensionless, rugosity factor =  $A_r/A_g$ , the ratio between the real and the geometric surface areas of the gold electrode used [198]

\*\* dimensionless,  $f$  = fractional area =  $A_a/A_g$ , the ratio between active and geometric areas of NEEs, calculated considering the pore diameter equal to 30 nm, as declared by the producer, or equal to 50 nm as a mean value calculated from the SEM measurements

**Table 1-** Comparison of the mean peak currents for the electrochemical oxidation of cysteamine amongst several NEE assemblies using a commercial gold electrode, a conventional NEE and NEE/SPS. Two different pore diameters (therefore diameters of a single nanoelectrode) are considered. Cysteamine oxidation performed at +800 mV vs Pt in a two-electrode configuration.

	sensors configurations			
	GOx/GA/MPE/NEE data from reference [214]	GOx/EDM/NEE/SPS	PANI/GOx/NEE/SPS	GOx/CYS/Au SPE
Explored range (mM)	Not reported	0.0075--31	0.019--20	0.2--20
Linearity range (mM)	up to 30	0.1--31	0.1--20	1--20
Sensitivity (nA mM <sup>-1</sup> )	110	35	18	0.9
reproducibility (%) *	3.7 (n=38)	3.9 (n=35)	4.4 (n=35)	14.2 (n=28)
detection limits (mM)	0.20	0,15	0,15	1.00
K <sub>m(app)</sub> (mM)	13.7	<b>14.9</b>	<b>8.9</b>	Not measured
shelf stability (days)	Not reported	20	15	2

\* 0.5 mM glucose injected *n* times

**Table 2-** Comparison of the analytical performances of different gold based biosensor for detection of glucose. *GOx/GA/MPE/NEE*: enzyme covalently immobilized on gold nanoelectrodes by means of a mercapto-compound coupling agent [214]; *GOx/EDM/NEE/SPS*: enzyme covalently immobilized via cysteamine electrodeposited multilayers and glutaraldehyde on gold nanoelectrodes ensemble sensor; *PANI/GOx/NEE/SPS*: enzyme covalently immobilized via amino propyl triethoxysilane and glutaraldehyde, polyaniline grown on gold nanodisks; *GOx/CYS/Au SPE*: enzyme covalently immobilized via electrodeposited cysteamine on a commercially available gold printed electrode (BVT Technologies, CZ).

## References:

1. a) Nalwa HS, editor. *Handbook of nanostructured biomaterials and their applications in nanobiotechnology*. American Scientific Publishers; 2005. ISBN 1-58883-004-7; b) Guozhong Cao. *Nanostructures and nanomaterials, Synthesis, Properties and Applications*. London: Imperial College press; 2004. ISBN1-86094-415-9.
2. Nirmal M, Norris DJ, Kuno M, Bawendi MG, Efros AL, Rosen M. Observation of the dark exciton in CdSe quantum dots. *Phys. Rev. Letters* 1995; **75(20)**: 3728-3731.
3. Alivisatos AP. Perspectives on the physical chemistry of semiconductor nanocrystals. *J. Phys. Chem.* 1996; **100(31)**: 13226-13239.
4. Alivisatos AP. Nanocrystals: Building block for modern materials design. *Endeavour* 1997; **21(2)**: 56-60.
5. Smalley RE, Yakobson BI. The future of fullerenes. *Solid State Comm.* 1998; **107(11)**: 597-606.
6. Bruchez M, Moronne M, Gin P, Weiss S, Alivisatos AP. Semiconductor nanocrystals as fluorescent biological labels. *Science* 1998; **281(5385)**: 2013-2016.
7. Williamson AJ, Zunger A. InAs quantum dots: predicted electronic structure of free-standing versus GaAs-embedded structures. *Physical Review B-Condens Matter* 1999; **59(24)**: 15819-15824.
8. Zhong CJ, Zheng WX, Leibowitz FL. Electrode nanomaterials self-assembled from thiolate encapsulated gold nanocrystals. *Electrochemistry Comm.* 1999; **1(2)**: 72-77.
9. Dubertret B, Calame M, Libchaber AJ. Single mismatch detection using gold-quenched fluorescent oligonucleotides. *Nature Biotechnology* 2001; **19(4)**: 365-370.
10. Zhang B, Liu C, Cheng HM, Cai QK. Progress in carbon nanotubes filled with foreign substances. *New Carbon Materials* 2003; **18(3)**: 174-180.
11. Lu Q, Moore JM, Huang G, Mount AS, Rao AM, Larcom LL, Ke PC. RNA polymer translocation with single-walled carbon nanotubes. *Nano Letters* 2004; **4(12)**: 2473-2477.
12. Guan WJ, Li Y, Chen YQ, Zhang XB, Hu GQ. Glucose biosensor based on multiwall carbon nanotubes and screen printed carbon electrodes. *Bios. and Bioelectronics* 2005; **21(3)**: 508-512.
13. Vastarella W, Nicastrì R. Enzyme/semiconductor nanoclusters combined systems for novel amperometric biosensors. *Talanta* 2005; **66**: 627-633.
14. Gouma P, Kalyanasundaram K, Bishop A. Electrospun single-crystal MoO<sub>3</sub> nanowires for biochemistry sensing probes. *J. Mater. Res.* 2006; **21(11)**: 2904-2910.
15. Reches M, Gasit E. Molecular self-assembly of peptide nanostructures: mechanism of association and potential uses. *Curr. Nanoscience* 2006; **2(2)**: 105-111.
16. Zhang HM, Quan X, Chen S, Zhao HM. Fabrication and characterization of silica-titania nanotubes composite membrane with photocatalytic capability. *Environmental Sci. & Technology* 2006; **40(19)**: 6104-6109.
17. Bavykin DV, Friedrich JM, Walsch FC. Protonated titanates and TiO<sub>2</sub> nanostructured materials: synthesis, properties, and applications. *Adv. Mater.* 2006; **18(21)**: 2807-2824.

18. Avouris P, Chen J. Nanotube electronics and optoelectronics. *Mater. Today* 2006; **9(10)**: 46-54.
19. Ago H, Uchimura E, Saito T, Ohshima S, Ishigami N, Tsuji M, Yumura M, Miyake M. Mechanical immobilization of *HeLa* cells on aligned carbon nanotube array. *Mater. Letters* 2006; **60(29-30)**: 3851-3854.
20. Corzilius B, Gembus A, Weiden N, Dinse KP, Hata K. EPR characterization of catalyst-free SWNT and N@C-60 based peapods. *Physica Status Solidi B-Basic Solid State Physics* 2006; **243(13)**: 3273-3276.
21. Ponce-de-Leon C, Bavykin DV, Walsch FC. The oxidation of borohydride ion at titanate nanotube supported gold electrodes. *Electrochemistry Comm.* 2006; **8(10)**: 1655-1660.
22. Chen L, Lu GX. Direct electrochemistry and electroanalysis of hybrid film assembled by polyelectrolyte-surfactant polymer, carbon nanotubes and hemoglobin. *J. Electroanal. Chem.* 2006; **597(1)**: 51-59.
23. Penner RM, Martin CR. Preparation and electrochemical characterization of ultramicroelectrode ensembles. *Anal. Chem.* 1987; **59(21)**: 2625-2630.
24. Cheng IF, Martin CR. Ultramicrodisk electrode ensembles prepared by incorporating carbon paste into a microporous host membrane. *Anal. Chem.* 1988; **60(19)**: 2163-2165.
25. Menon VP, Martin CR. Fabrication and evaluation of nanoelectrode ensembles. *Anal. Chem.* 1995; **67(13)**: 1920-1928.
26. Martin CR, Mitchell DT. *Electroanalytical Chemistry, a Series of Advances*. Vol. 21, New York: Marcell Dekker; 1999.
27. Martin CR, Mitchell DT. Nanomaterials in analytical chemistry. *Anal. Chem.* 1998; **70(9)**: 322 A-327 A.
28. Almawlawi D, Liu CZ, Moskovits M. Nanowires formed in anodic oxide nanotemplates. *J. Mater. Res.* 1994; **9(4)**: 1014-1018.
29. Li J, Moskovits M, Haslett TL. Nanoscale electroless metal deposition in aligned carbon nanotubes. *Chem. Mater.* 1998; **10(7)**: 1963-1967.
30. Davydov DN, Haruyama J, Routkevitch D, Statt BW, Ellis D, Moskovits M, Xu JM. Nonlithographic nanowire-array tunnel device: fabrication, zero-bias anomalies, and Coulomb blockade. *Phys. Rev. B* 1998; **57(21)**: 13550-13553.
31. Li J, Papadopoulos C, Xu JM, Moskovits M. Highly ordered carbon nanotube arrays for electronics applications. *Appl. Phys. Lett.* 1999; **75(3)**: 367-369.
32. Preston CK, Moskovits M. Optical characterization of anodic aluminum oxide films containing electrochemically deposited metal particles. *J. Phys. Chem* 1993; **97(32)**: 8495-8503.
33. Routkevitch D, Bigioni T, Moskovits M, Xu JM. Electrochemical fabrication of CdS nanowire arrays in porous anodic aluminum oxide templates. *J. Phys. Chem.* 1996; **100(33)**: 14037-14047.
34. Ji CX, Searson PC. Synthesis and characterization of nanoporous gold nanowires. *J. Phys. Chem. B* 2003; **107(19)**: 4494-4499.

35. Lewandowski EP, Searson PC, Stebe KJ. Orientation of a nanocylinder at a fluid interface. *J. Phys. Chem. B* 2006; **110(9)**: 4283-4290.
36. Searson PC, Cammarata RC, Chien CL. Electrochemical processing of metallic nanowire arrays and nanocomposites. *J. Electronic Mater.* 1995; **24(8)**: 955-960.
37. Whitney TM, Jiang JS, Searson PC, Chien CL. Fabrication and magnetic properties of arrays of metallic nanowires. *Science* 1993; **261(5126)**: 1316-1319.
38. Liu K, Nagodawithana K, Searson PC, Chien CL. Perpendicular giant magnetoresistance of multilayered Co/Cu nanowires. *Phys. Rev. B* 1995; **51(11)**: 7381-7384.
39. Liu K, Chien CL, Searson PC, Kui YZ. Structural and magneto-transport properties of electrodeposited bismuth nanowires. *Appl. Phys. Lett.* 1998; **73(10)**: 1436-1438.
40. Liu K, Chien CL, Searson PC. Finite-size effects in bismuth nanowires. *Phys. Rev. B* 1998; **58(22)**: 14681-14684.
41. Deckman HWD, Dunsmuir JH. Natural lithography. *Appl. Phys. Lett.* 1982; **41**: 377-379.
42. Hanarp P, Sutherland DS, Gold J, Kasemo B. Nanostructured biomaterials surfaces prepared by colloidal lithography. *Nanostruct. Mater.* 1999; **12**: 429-432.
43. Hulteen JC, Van Duyne RP. Nanosphere lithography: a materials general fabrication process for periodic particle array surfaces. *J. Vacuum Sci. Technology A: Vacuum, Surfaces, and Films* 1995; **13(3)**: 1553-1558.
44. Andersson AS, Olsson P, Lidberg U, Sutherland D. The effects of continuous and discontinuous groove edges on cell shape and alignment. *Exp. Cell Res.* 2003; **288**: 177-188.
45. Andersson AS, Backhed F, von Euler A, Richter-Dahlfors A, Sutherland D, Kasemo B. Nanoscale features influence epithelial cell morphology and cytokine production. *Biomaterials* 2003; **24**: 3427-3436.
46. Dalby MJ, Riehle MO, Sutherland DS, Agheli H, Curtis ASG. Morphological and microarray analysis of human fibroblasts cultured on nanocolumns produced by colloidal lithography. *Eur. Cells Mater.* 2005; **9**: 1-8.
47. Haes AJ, van Duyne RP. A nanoscale optical biosensor: sensitivity and selectivity of an approach based on the localized surface plasmon resonance spectroscopy of triangular silver nanoparticles. *J. Am. Chem. Soc.* 2002; **124**: 10596-10604.
48. Haes AJ, Hall WP, Chang L, Klein WL, van Duyne RP. A localized surface plasmon resonance biosensor: first steps toward an assay for alzheimer's disease. *Nano Lett.* 2004; **4**: 1029-1034.
49. Haynes CL, Van Duyne RP. Nanosphere lithography: a versatile nanofabrication tool for studies of size-dependent nanoparticle optics. *J. Phys. Chem. B* 2001; **105(24)**: 5599-5611.
50. McFarland AD, Van Duyne RP. Single silver nanoparticles as real-time optical sensors with zeptomole sensitivity. *Nano Lett.* 2003; **3**: 1057-1062.
51. Cheng S, Lu S, Li C, Chang Y, Huang C, Chen H. Fabrication of periodic nickel silicide nanodot arrays using nanosphere lithography. *Thin Solid Films* 2006; **494(1-2)**: 307-310.
52. Bhaviripudi S, Reina A, Qi JF, Kong J, Belcher AM. Block-copolymer assisted synthesis of arrays

- of metal nanoparticles and their catalytic activities for the growth of SWNTs. *Nanotechnology* 2006; **17**: 5080-5086.
53. Yang Z, Huck WT, Clarke SM, Tajbakhsh AR, Terentjev EM. Shape-memory nanoparticles from inherently non-spherical polymer colloids. *Nat. Mater.* 2005; **4**: 486-490.
  54. Ng V, Lee YV, Chen BT, Adeyeye AO. Nanostructure array fabrication with temperature-controlled self-assembly techniques. *Nanotechnology* 2002; **13**: 554-558.
  55. Ray MA, Kim H, Jia L. Dynamic self-assembly of polymer colloids to form linear patterns. *Langmuir* 2001; **21**: 4786-4789.
  56. Sonvico F, Dubernet C, Colombo P, Couvreur P. Metallic colloid nanotechnology, applications in diagnosis and therapeutics. *Curr. Pharm. Des.* 2005; **11**: 2095-2105.
  57. Laurent G, Felidj N, Lau Truong S, Aubard J, Levi G, Krenn JR, Hohenau A, Leitner A, Aussenegg FR. Imaging surface plasmon of gold nanoparticle arrays by far-field Raman scattering. *Nano Lett.* 2005; **5**: 253-258.
  58. Schlotterbeck U, Aymonier C, Thomann R, Hofmeister H, Tromp M, Richtering W, Mecking S. Shape-selective synthesis of palladium nanoparticles stabilized by highly branched amphiphilic polymers. *Adv. Funct. Mater.* 2004; **14**: 999-1004.
  59. Andersson A, Glasmästar K, Hanarp P, Seantier B, Sutherland DS. Patterning colloidal monolayer films using microcontact particle stripping. *Nanotechnology* 2007; **18(20)**: 205303.
  60. Hanarp P, Sutherland DS, Gold J, Kasemo B. Control of nanoparticle film structure for colloidal lithography. *Colloids and Surfaces A: Physicochemical and Engineering Aspects* 2003; **214 (1-3)**: 23-26.
  61. Silván MM, Hernández MA, Costa VT, Palma RJM, Duart JMM. Structured porous silicon sub-micrometer wells grown by colloidal lithography. *Europhysics Letters (EPL)* 2006; **76(4)**: 690-695.
  62. Yap F, Zhang Y. Protein and cell micropatterning and its integration with micro/nanoparticles assembly. *Bios. and Bioelectronics* 2007; **22(6)**: 775-778.
  63. Yap FL, Zhang Y. Assembly of polystyrene microspheres and its application in cell micropatterning. *Biomaterials* 2007; **28(14)**: 2328-2338.
  64. Juillerat F, Solak HH, Bowen P, Hofmann H. Fabrication of large-area ordered arrays of nanoparticles on patterned substrates. *Nanotechnology* 2005; **16(8)**: 1311-1316.
  65. Nath N, Chilkoti A. A colorimetric colloidal gold sensor to interrogate biomolecular interactions in real-time on a surface. *Anal. Chem.* 2002; **74**: 504-509.
  66. Städler B, Solak HH, Frerker S, Bonroy K, Frederix F, VUČIĆ L, Grandin HM. Nanopatterning of gold colloids for label-free biosensing. *Nanotechnology* 2007; **18(15)**: 155306.
  67. Satriano C, Messina G, Carnazza S, Guglielmino S, Marletta G. Bacterial adhesion onto nanopatterned polymer surfaces. *Mater. Science and Engineering: C* 2006; **26(5-7)**: 942-946.
  68. Valsesia A, Meziani T, Bretagnol F, Colpo P, Leccone G, Rossi F. Plasma assisted production of chemical nano-patterns by nano-sphere lithography: application to bio-interfaces. *J. of Physics D: Applied Physics* 2007; **40(8)**: 2341-2347.

69. Dalby MJ, Riehle MO, Sutherland DS, Agheli H, Curtis ASG. Changes in fibroblast morphology in response to nano-columns produced by colloidal lithography. *Biomaterials* 2004; **25(23)**: 5415-5422.
70. Norman J, Desai T. Methods for fabrication of nanoscale topography for tissue engineering scaffolds. *Annals of Biomedical Engineering* 2006; **34(1)**: 89-101.
71. Antelmi DA, Spalla O. Adsorption of nanolatex particles to mineral surfaces of variable surface charge. *Langmuir* 1999; **15**: 7478-7489.
72. Serizawa T, Kamimura S, Akashi M. Electrostatic adsorption of polystyrene particles with different surface charges onto the surface of an ultrathin polymer film. *Colloids Surf. A* 2000; **164**: 237-245.
73. Serizawa T, Takeshita H, Akashi M. Electrostatic adsorption of polystyrene nanospheres onto the surface of an ultrathin polymer film prepared by using an alternate adsorption technique. *Langmuir* 1998; **14**: 4088-4094.
74. Yang SM, Jang SG, Choi DG, Kim S, Yu HK. Nanomachining by colloidal lithography. *Small* 2006; **2**: 458-475.
75. Wood M. Colloidal lithography and current fabrication techniques producing in-plane nanotopography for biological applications. *Journal of The Royal Society Interface* 2007; **4(12)**: 1-17.
76. van Blaaderen A, Ruel R, Wiltzius P. Template-directed colloidal crystallization. *Nature* 1997; **285**: 321-324.
77. Bailey RC, Stevenson KJ, Hupp JT. Assembly of micropatterned colloidal gold thin films via microtransfer molding and electrophoretic deposition. *Adv. Mater.* 2000; **12**: 1930-1934.
78. Xia D, Brueck SRJ. A facile approach to directed assembly of patterns of nanoparticles using interference lithography and spin coating. *Nano Lett.* 2004; **4**: 1295-1299.
79. Xia D, Biswas A, Li D, Brueck SRJ. Directed self-assembly of silica nanoparticles into nanometer-scale patterned surfaces using spin-coating. *Adv. Mater.* 2004; **16**: 1427-1432.
80. Wood MA, Meredith DO, Owen GHR, Richards RG, Riehle MO. Utilising atomic number contrast for FESEM imaging of colloidal nanotopography underlying biological cells. *Nanotechnology* 2005; **16**: 1433-1439.
81. Wood MA, Wilkinson CDW, Curtis ASG. The effects of colloidal nanotopography on initial fibroblast adhesion and morphology. *IEEE Trans. Nanobiosci.* 2006; **5(1)**: 20-31.
82. Haginoya C, Ishibashi M, Koike K. Nanostructure array fabrication with a size-controllable natural lithography. *Appl. Phys. Lett.* 1997; **71**: 2934-2936.
83. Denis FA, Hanarp P, Sutherland DS, Dufrene YF. Nanoscale chemical patterns fabricated by using colloidal lithography and self-assembled monolayers. *Langmuir* 2004; **20**: 9335-9339.
84. Wood MA, Riehle M, Wilkinson CDW. Patterning colloidal nanotopographies. *Nanotechnology* 2002; **13**: 605-609.
85. Lewis PA, Ahmed H. Nanopillars formed with a colloidal gold etch mask. *J. Vac. Sci. Tech. B* 1999; **17**: 3239-3234.

86. Lewis PA, Ahmed H, Sato T. Silicon nanopillars formed with colloidal particle masking. *J. Vac. Sci. Tech. B* 1998; **16**: 2938-2941.
87. Cheung CL, Nikoli RJ, Reinhardt CE, Wang TF. Fabrication of nanopillars by nanosphere lithography. *Nanotechnology* 2006; **17(5)**: 1339-1343.
88. Denis FA, Hanarp P, Sutherland DS, Dufrene YF. Fabrication of nanostructured polymer surfaces using colloidal lithography and spin-coating. *Nano Lett.* 2002; **2**: 1419-1425.
89. Werdinius C, Osterlund CL, Kasemo B. Nanofabrication of planar model catalysts by colloidal lithography: Pt/ceria and pt/alumina. *Langmuir* 2003; **19**: 458-468.
90. Prikulis J, Hanarp P, Olofsson L, Sutherland DS, Kall M. Optical spectroscopy of nanometric holes in thin gold films. *Nano Lett.* 2004; **4**: 1003-1007.
91. Whitney AV, Myers BD, van Duyne RP. Sub-100 nm triangular nanopores fabricated with the reactive ion etching variant of nanosphere lithography and angle-resolved nanosphere lithography. *Nano Lett.* 2004; **4**: 1507-1511.
92. Jiang P, McFarland MJ. Wafer-scale periodic nanohole arrays templated from two-dimensional nonclose-packed colloidal crystals. *J. Am. Chem. Soc.* 2005; **127**: 3710-3711.
93. Aizpurua J, Hanarp P, Sutherland DS, Kall M, Bryant GW, de Abajo FJG. Optical properties of gold nanorings. *Phys. Rev. Lett.* 2003; **90(5)**: 057401.
94. Hovis JS, Boxer SG. Patterning barriers to lateral diffusion in supported lipid membranes by blotting and stamping. *Langmuir* 2000; **16**: 894-897.
95. Zheng Y, Wang S, Huan A, Wang Y. Fabrication of large area ordered metal nanoring arrays for nanoscale optical sensors. *J. Non-Crystalline Solids* 2006; **352(23-25)**: 2532-2535.
96. Michel R, Reviakine I, Sutherland D, Fokas C, Csucs G, Danuser G, Spencer N, Textor M. A novel approach to produce biologically relevant chemical patterns at the nanometer scale: selective molecular assembly patterning combined with colloidal lithography. *Langmuir* 2002; **18**: 8580-8586.
97. Qin K, Li Y. Mechanisms of particle removal from silicon wafer surface in wet chemical cleaning process. *J. Colloid Interface Sci.* 2003; **261**: 569-574.
98. Brétagnot F, Ceriotti L, Valsesia A, Sasaki T, Ceccone G, Gilliland D, Colpo P, Rossi F. Fabrication of functional nano-patterned surfaces by a combination of plasma processes and electron-beam lithography. *Nanotechnology* 2007; **18(13)**: 135303.
99. Nakagawa M, Oh SK, Ichimura K. Photopatterning and visualization of adsorbed monolayers of bis(1-benzyl-4-pyridinio)ethylene moieties. *Adv. Mater.* 2000; **12**: 403-407.
100. Bale M, Turner AJ, Palmer RE. Fabrication of ordered arrays of silicon nanopillars at selected sites. *J. Phys. D: Appl. Phys.* 2002; **35**: L11-14.
101. Fudouzi H, Kobayashi M, Shinya N. Assembling 100 nm scale particles by an electrostatic potential field. *J. Nanopart. Res.* 2001; **3**: 193-200.
102. Aizenberg J, Braun PV, Wiltzius P. Patterned colloidal deposition controlled by electrostatic and capillary forces. *Phys. Rev. Lett.* 2000; **84**: 2997-3000.

103. Himmelhaus M, Takei H. Self-assembly of polystyrene nano particles into patterns of random-close-packed monolayers via chemically induced adsorption. *Phys. Chem. Chem. Phys.* 2002; **4**: 496-506.
104. Park MC, Chaikin PM, Register RA, Adamson DH. Large area dense nanoscale patterning of arbitrary surfaces. *Appl. Phys. Lett.* 2001; **79**: 257-259.
105. Kim SO, Solak HH, Stoykovich MP, Ferrier NJ, De Pablo JJ, Nealey PF. Epitaxial self-assembly of block copolymers on lithographically defined nanopatterned substrates. *Nature* 2003; **424**: 411.
106. Segalman RA. Patterning with block copolymer thin films. *Mater. Science and Engineering R* 2005; **48**: 191-226.
107. Hamley IW. Nanostructure fabrication using block copolymers. *Nanotechnology* 2003; **14**: R39-54.
108. Glass R, Moller M, Spatz JP. Micellar nanolithography. *Nanotechnology* 2003; **14**: 1153-1160.
109. Glass R, Arnold M, Cavalcanti-Adam E, Blümmel C, Haferkemper C, Dodd C, Spatz JP. Block copolymer micelle nanolithography on non-conductive substrates. *New J. Physics* 2004; **6**: 101-117.
110. Arnold M, Cavalcanti-Adam E, Glass R, Blümmel J, Eck W, Kantlehner M, Kessler H, Spatz JP. Activation of integrin function by nanopatterned adhesive interfaces. *Chem. Phys. Chem.* 2004; **5**: 383-388.
111. Cavalcanti-Adam E, Micoulet A, Blümmel J, Aurenheimer J, Kessler H, Spatz JP. Lateral spacing of integrin ligands influences cell spreading and focal adhesion assembly. *Eur. J. Cell Biol.* 2006; **85**: 219-224.
112. Curtis AS. The potential for the use of nanofeaturing in medical devices. *Expert Rev. Med. Dev.* 2005; **2**: 293-301.
113. Agheli H, Malmstrom J, Larsson E, Textor M, Sutherland D. Large area protein nanopatterning for biological applications. *Nano Lett.* 2006; **6(6)**: 1165-1171.
114. Li JR, Henry GC, Garno JC. Fabrication of nanopatterned films of bovine serum albumin and staphylococcal protein A using latex particle lithography. *Analyst* 2006; **131(2)**: 244-250.
115. Cai Y, Ocko B. Large scale fabrication of protein nanoarrays based on nanosphere lithography. *Langmuir* 2005; **21(20)**: 9274-9279.
116. Kumar N, Parajuli O, Hahm J. Two-dimensionally self-arranged protein nanoarrays on diblock copolymer templates. *J. Phys. Chem. B* 2007; **111(17)**: 4581-4587.
117. Kumar N, Parajuli O, Dorfman A, Kipp D, Hahm J. Activity study of self-assembled proteins on nanoscale diblock copolymer templates. *Langmuir* 2007; **23(14)**: 7416-7422.
118. Sutherland DS, Broberg M, Nygren H, Kasemo B. Influence of nanoscale surface topography and chemistry on the functional behaviour of an adsorbed model macromolecule. *Macromol. Biosci.* 2001; **1**: 270-273.
119. Silva GA. Neuroscience nanotechnology: progress, opportunities and challenges. *Nat. Rev. Neurosci.* 2006; **7**: 65-74.

120. Busch K, Tampe R. Single molecule research on surfaces: from analytics to construction and back. *Mol. Biotechnol.* 2001; **82**: 3-24.
121. Wolfram T, Belz F, Schoen T, Spart JP. Site-specific presentation of single recombinant proteins in defined nanoarrays. *Biointerphases* 2007; **2(1)**: 44-48.
122. Vertegel AA, Siegel RW, Dordick JS. Silica nanoparticle size influences the structure and enzymatic activity of adsorbed lysozyme. *Langmuir* 2004; **20**: 6800-6807.
123. Lundqvist M, Sethson I, Jonsson BH. Protein adsorption onto silica nanoparticles: conformational changes depend on the particles' curvature and the protein stability. *Langmuir* 2004; **20**: 10639-10647.
124. Link S, El-Sayed MA. Spectral properties and relaxation dynamics of surface plasmon electronic oscillations in gold and silver nanodots and nanorods. *J. Phys. Chem. B* 1999; **103(40)**: 8410-8426.
125. El-Sayed MA. Some interesting properties of metals confined in time and nanometer space of different shapes. *Acc. Chem. Res.* 2001; **34(4)**: 257-264.
126. Hirsch LR, Jackson JB, Lee A, Halas NJ, West JL. A whole blood immunoassay using gold nanoshells. *Anal. Chem.* 2003; **75(10)**: 2377-2381.
127. Haes AJ, Van Duyne RP. Silver nanoparticles behave as ultrasensitive biosensors. *Laser Focus World* 2003; **39**: 153-156.
128. Kreibig U, Vollmer M. *Optical properties of metal clusters*. Vol. **25**. Springer, 1995: 532.
129. Zhang X, Whitney AV, Zhao J, Hicks EM, van Duyne RP, Richard P. Advances in contemporary nanosphere lithographic techniques. *J. Nnosci. Nanotec.* 2006; **6(7)**: 1920-1934.
130. Haynes CHL, McFarland AD, Smith MT, Hulteen JC, van Duyne RP. Angle-resolved nanosphere lithography: manipulation of nanoparticle size, shape, and interparticle spacing. *J. Phys. Chem. B* 2002; **106(8)**: 1898-1902.
131. Taton TA, Mirkin CA, Letsinger RL. Scanometric DNA array detection with nanoparticle probes. *Science* 2002; **289(5485)**: 1757-1760.
132. Storhoff JJ, Elghanian R, Mirkin CA, Letsinger RL. Stability of DNA-modified gold nanoparticles. *Langmuir* 2002; **18(17)**: 6666-6670.
133. Elghanian R, Storhoff JJ, Mucic RC, Letsinger RL, Mirkin CA. Selective colorimetric detection of polynucleotides based on the distance-dependent optical properties of gold nanoparticles. *Science* 1997; **227(5329)**: 1078-1081.
134. Riboh JC, Haes AJ, McFarland AD, Yonzon CR, Van Duyne RP. A nanoscale optical biosensor: real time immunoassay and nanoparticle adhesion. *J. Phys. Chem. B* 2003; **107**: 1772-1780.
135. Haynes CL, Van Duyne RP. Nanosphere lithography: a versatile nanofabrication tool for studies of size-dependent nanoparticle optics. *J. Phys. Chem. B* 2001; **105**: 5599-5601.
136. Haes AJ, Zou S, Schatz GC, Van Duyne RP. A nanoscale optical biosensor: the long range distance dependence of the localized surface plasmon resonance of noble metal nanoparticles. *J. Phys. Chem. B* 2004; **108**: 109-116.

137. Yonzon CR, Stuart DA, Zhang X, McFarland AD, Haynes CL, Van Duyne RP. Towards advanced chemical and biological nanosensors- An overview. *Talanta* 2005; **67(3)**: 438-448.
138. Hanarp P, Käll M, Sutherland DS. Optical properties of short range ordered arrays of nanometer gold disks prepared by colloidal lithography. *J. Phys. Chem. B* 2003; **107**: 5768-5772.
139. Foss JCA, Hornyak GL, Stockert JA, Martin CR. Template synthesized nanoscopic gold particles- optical spectra and the effects of particle size and shape. *J. Phys. Chem.* 1994; **98(11)**: 2963-2971.
140. Hornyak GL, Phani KLN, Kunkel DL, Menon VP, Martin CR. Fabrication, characterization and optical theory of aluminum nanometal nanoporous membrane thin film composites. *Nanostr. Mater.* 1995; **6(5-8)**: 839-842.
141. Patemarakis G. Transport phenomena inside the pores involved in the kinetics and mechanism of growth of porous anodic Al<sub>2</sub>O<sub>3</sub> films on aluminium. *J. Electroanal. Chem.* 1996; **404(1)**: 69-76.
142. Zhang ZB, Gekhtman D, Dresselhaus MS, Ying JY. Processing and characterization of single-crystalline ultrafine bismuth nanowires. *Chem. Mater.* 1999; **11(7)**: 1659-1665.
143. Masuda H, Hasegawa F, Ono S. Self-ordering of cell arrangement of anodic porous alumina formed in sulfuric acid solution. *J. Electrochem. Soc.* 1997; **144(5)**: L127-130.
144. Cheng GS, Zhang LD, Zhu XG, Chen SH, Li Y, Zhu Y, Fei GT. Synthesis of orderly nanostructure of crystalline GaN nanoparticles on anodic porous alumina membrane. *Nanostr. Mater.* 1999; **11(3)**: 421-426.
145. Mozalev A, Poznyak A, Mozaleva I, Hassel AW. The voltage-time behaviour for porous anodizing of aluminium in a fluoride-containing oxalic acid electrolyte. *Electrochem. Comm.* 2001; **3(6)**: 299-305.
146. Brumlik CJ, Menon VP, Martin CR. Template synthesis of metal microtubule ensembles utilizing chemical, electrochemical, and vacuum deposition techniques. *J. Mater. Res.* 1994; **9(5)**: 1174-1183.
147. Hoyer P, Masuda H. Electrodeposited nanoporous TiO<sub>2</sub> film by a two-step replication process from anodic porous alumina. *J. Mater. Sci. Lett.* 1996; **15(14)**: 1228-1230.
148. Shawaqfeh AT, Baltus RE. Growth kinetics and morphology of porous anodic alumina films formed using phosphoric acid. *J. Electrochem. Soc.* 1998; **145(8)**: 2699-2706.
149. Cheng GS, Zhang LD, Zhu Y, Fei GT, Li L, Mo CM, Mao YQ. Large scale synthesis of single crystalline gallium nitride nanowires. *Appl. Phys. Lett.* 1999; **75(16)**: 2455-2457.
150. Shawaqfeh AT, Baltus RE. Fabrication and characterization of single layer and multilayer anodic alumina membrane. *J. Memb. Sci.* 1999; **157(2)**: 147-158.
151. Bocchetta P, Sunseri C, Bottino A, Capannelli G, Chiavarotti G, Piazza S, Quarto F. Asymmetric alumina membranes electrochemically formed in oxalic acid solution. *J. Appl. Electrochem.* 2002; **32(9)**: 977-985.
152. Piao Y, Lim H, Chang JY, Lee WY, Kim H. Nanostructured materials prepared by use of ordered porous alumina. *Electrochim. Acta* 2005; **50(15)**: 2997-3013.

153. Ugo P, Moretto LM. *Metal deposition*. In: Zoski CG editor. *Handbook of Electrochemistry*. Amsterdam: Elsevier Science; 2007. Chapter **16**, Section **16.2**: 678-709.
154. Hornyak GL, Patrissi CJ, Martin CR. Fabrication, characterization, and optical properties of gold nanoparticle/porous alumina composites: the nonscattering Maxwell-Garnett limit. *J. Phys. Chem. B* 1997; **101(9)**: 1548-1555.
155. Furneaux RC, Rigby WR, Davidsons AP. *Porous films and methods forming them*. US patent number 4,687,551. 1987.
156. Parpaleix T, Laval JM, Majda M, Bourdillon C. Potentiometric and voltammetric investigations of H<sub>2</sub>/H<sup>+</sup> catalysis by periplasmic hydrogenase from desulfovibrio-gigas immobilized at the electrode surface in an amphiphilic bilayer assembly. *Anal. Chem.* 1992; **64(6)**, 641-646.
157. Mozalev A, Magaino S, Imai H. The formation of nanoporous membranes from anodically oxidized aluminium and their application to Li rechargeable batteries. *Electrochim. Acta* 2001; **46(18)**: 2825-2834.
158. Tian M, Xu S, Wang JG, Kumar N, Wertz E, Li Q, Campbell PM, Chan MHW, Mallouk TE. Penetrating the oxide barrier in situ and separating freestanding porous anodic alumina films in one step. *Nano Lett.* 2005; **5(4)**: 697-703.
159. Harrell CC, Lee SB, Martin CR. Synthetic single nanopore and nanotube membranes. *Anal. Chem.* 2003; **75(24)**: 6861-6867.
160. Trautman C, Bruchle W, Spohr R, Vetter J, Angert N. Pore geometry of etched ion tracks in polyimide. *Nucl. Instrum. Methods Phys. Res. B* 1996; **111(1-2)**: 70-74.
161. Apel P. Track etching technique in membrane technology. *Radiat. Meas.* 2001; **34(1-6)**: 559-566.
162. Scopece P, Baker LA, Ugo P, Martin CR. Conical nanopore membranes: solvent shaping of nanopores. *Nanotechnology* 2006; **17(15)**: 3951-3956.
163. Apel PY, Korchev YE, Siwy Z, Spohr R, Yoshida M. Diode-like single ion track membrane prepared by electro-stopping. *Nucl. Instrum. Methods Phys. Res. B* 2001; **184(3)**: 337-346.
164. Siwy Z, Apel P, Baur D, Dobrev DD, Korchev YE, Neumann R, Spohr R, Trautmann C, Voss KO. Preparation of synthetic nanopores with transport properties analogous to biological channels. *Surf. Sci.* 2003; **532**: 1061-1066.
165. Masuda H, Tanaka H, Baba N. Preparation of microporous gold film by two step replicating process using anodic alumina as template. *Bull. Chem. Soc. Japan* 1993; **66(1)**: 305-311.
166. Kautek W, Reetz S, Pentzien S. Template electrodeposition of nanowire arrays on gold foils fabricated by pulsed-laser deposition. *Electrochim. Acta* 1995; **40(10)**: 1461-1468.
167. Schönenberger C, vanderZande BMI, Fokink LGJ, Henny M, Schmid C, Krüger M, Bachtold A, Huber R, Birk H, Staufer U. Template synthesis of nanowires in porous polycarbonate membranes: electrochemistry and morphology. *J. Phys. Chem. B* 1997; **101(28)**: 5497-5505.
168. Tian M, Wang JU, Kurtz J, Mallouk TE, Chan MHW. Electrochemical growth of single-crystal metal nanowires via a two-dimensional nucleation and growth mechanism. *Nano Lett.* 2003; **3(7)**: 919-923.

169. Zhao Y, Guo YG, Zhang YL, Jiao K. Fabrication and characterization of highly ordered Pt nanotubule arrays. *Phys. Chem. Chemical Phys.* 2004; **6(8)**: 1766-1768.
170. Fukunaka Y, Motoyama M, Konishi Y, Ishii R. Producing shape-controlled metal nanowires and nanotubes by an electrochemical method. *Electrochem. Solid State Lett.* 2006; **9(3)**: C62-64.
171. Karim S, Toimil-Molares ME, Maurer F, Mische G, Ensinger W, Liu J, Cornelius TW, Neumann R. Synthesis of gold nanowires with controlled crystallographic characteristics. *Appl. Phys. A-Mater. Sci. Processing* 2006; **84(4)**: 403-407.
172. Gelves GA, Lin B, Sundararaj U, Haber JA. Low electrical percolation threshold of silver and copper nanowires in polystyrene composites. *Adv. Funct. Mater.* 2006; **16(18)**: 2423-2430.
173. Gelves GA, Murakami ZTM, Krantz MJ, Haber JA. Multigram synthesis of copper nanowires using AC electrodeposition into porous aluminium oxide templates. *J. Mater. Chem.* 2006; **16(30)**: 3075-3083.
174. Evans P, Hendren WR, Atkinson R, Wurtz GA, Dickson W, Zayats AV, Pollard RJ. Growth and properties of gold and nickel nanorods in thin film alumina. *Nanotechnology* 2006; **17(23)**: 5746-5753.
175. Lee UH, Lee JH, Jung DY, Kwon YU. High-density arrays of platinum nanostructures and their hierarchical patterns. *Adv. Mater.* 2006; **18(21)**: 2825-2828.
176. Xu LP, Yuan ZH, Zhang XG. Fabrication of multi-level branched metal nanowires by AAO template electrodeposition. *Chinese Sci. Bull.* 2006; **51(17)**: 2055-2058.
177. Ohgai T, Enculescu I, Zet C, Westerberg L, Hjort K, Spohr R, Neumann R. Magnetosensitive nickel nanowires fabricated by electrodeposition into multi- and single-ion track templates. *J. Applied Electrochem.* 2006; **36(10)**: 1157-1162.
178. Kazeminezhad I, Barnes AC, Holbrey JD, Seddon KR, Schwarzacher W. Templated electrodeposition of silver nanowires in a nanoporous polycarbonate membrane from a nonaqueous ionic liquid electrolyte. *Appl. Phys. A-Mater. Sci. Processing* 2007; **86(3)**: 373-375.
179. Han S, Chen HY, Chen CC, Yuan TN, Shih HC. Characterization of Ni nanowires after annealing. *Mater. Lett.* 2007; **61(4-5)**: 1105-1108.
180. Xu XJ, Fei GT, Wang XW, Jin Z, Yu WH, Zhang LD. Synthetic control of large area, ordered silver nanowires with different diameters. *Mater. Lett.* 2007; **61(1)**: 19-22.
181. Penner RM. *Metal deposition*. In: Zoski CG editor. *Handbook of Electrochemistry*. Amsterdam: Elsevier Science; 2007. Chapter **16**, Section **16.1**: 673-677.
182. Zhu JT, Jiang W. Fabrication of conductive metallized nanostructures from self-assembled amphiphilic triblock copolymer templates: nanospheres, nanowires, nanorings. *Mater. Chem. Phys.* 2007; **101(1)**: 56-62.
183. Williams WD, Giordano N. Fabrication of 80-A metal wires. *Rev. Sci. Instrum.* 1984; **55(3)**: 410-412.
184. Brumlik CJ, Martin CR, Tokuda K. Microhole array electrodes based on microporous alumina membranes. *Anal. Chem.* 1992; **64(10)**: 1201-1203.

185. van der Zande BMI, Böhmer MR, Fokkink LGJ, Schönenberger C. Colloidal dispersions of gold rods: synthesis and optical properties. *Langmuir* 2000; **16(2)**: 451-458.
186. Zhang XY, Zhang LD, Lei Y, Zhao LX, Mao YQ. Fabrication and characterization of highly ordered Au nanowire arrays. *J. Mater. Chem.* 2001; **11(6)**: 1732-1734.
187. Piraux L, Dubois S, Demoustier-Champagne S. Template synthesis of nanoscale materials using the membrane porosity. *Nucl. Instrum. Methods Phys. Res. B* 1997; **131(1-4)**: 357-363.
188. Chiriac H, Moga AE, Urse M, Óvári TA. Preparation and magnetic properties of electrodeposited magnetic nanowires. *Sens. Actuators A* 2003; **106(1-3)**: 348-351.
189. Verbeeck J, Lebedev OI, Van Tendeloo G, Cagnon L, Bougerol C, Tourillon G. Fe e Co nanowires and nanotubes synthesized by template electrodeposition- A HRTEM and EELS study. *J. Electrochem. Soc.* 2003; **150(10)**: E468-471.
190. Tourillon G, Pontonnier L, Levy JP, Langlais V. Electrochemically synthesized Co and Fe nanowires and nanotubes. *Electrochem. Solid State Lett.* 2000; **3(1)**: 20-23.
191. Zheng MJ, Li GH, Zhang XY, Huang SY, Lei Y, Zhang LD. Fabrication and structural characterization of large-scale uniform SnO<sub>2</sub> nanowire array embedded in anodic alumina membrane. *Chem. Mater.* 2001; **13(11)**: 3859-3861.
192. Platt M, Dryfe RAW, Roberts EPL. Electrodeposition of palladium nanoparticles at the liquid-liquid interface using porous alumina templates. *Electrochim. Acta* 2003; **48(20-22)**: 3037-3046.
193. Platt M, Dryfe RAW, Roberts EPL. Structural and electrochemical characterisation of Pt and Pd nanoparticles electrodeposited at the liquid/liquid interface. *Electrochim. Acta* 2004; **49(22-23)**: 3937-3945.
194. Tian ML, Wang JG, Snyder J, Kurtz J, Liu Y, Schiffer P, Mallouk TE, Chan MHW. Synthesis and characterization of superconducting single-crystal Sn nanowires. *Appl. Phys. Lett.* 2003; **83(8)**: 1620-1622.
195. Wang JG, Tian ML, Mallouk TE, Chan MHW. Microstructure and interdiffusion of template-synthesized Au/Sn/Au junction nanowires. *Nano Lett.* 2004; **4(7)**: 1313-1318.
196. Jirage KB, Hulteen JC, Martin CR. Effect of thiol chemisorption on the transport properties of gold nanotubule membranes. *Anal. Chem.* 1999; **71(21)**: 4913-4918.
197. Göring P, Pippel E, Hofmeister H, Wehrspohn RB, Steinhart M, Gösele U. Gold/carbon composite tubes and gold nanowires by impregnating templates with hydrogen tetrachloroaurate/acetone solutions. *Nano Lett.* 2004; **4(6)**: 1121-1125.
198. Vastarella W, Della Seta L, Masci A, Maly J, De Leo M, Moretto LM, Pilloton R. Biosensors based on gold nanoelectrode ensembles and screen printed electrodes. *Int. J. Environ. Anal. Chem.* 2007; **87(10-11)**: 701-714.
199. Lahav M, Sehayek T, Vaskevich A, Rubinstein I. Nanoparticle nanotubes. *Angew. Chem. Int. Ed.* 2003; **42(45)**: 5575-5579.
200. Barreca D, Gasparotto A, Maragno C, Tondello E. Synthesis of gold nanotubes by sputtering of gold into porous materials. *J. Nanosci. Nanotech.* 2005; **5(11)**: 1883-1886.

201. Liu J, Duan JL, Toimil-Molares E, Karim S, Cornelius TW, Dobrev D, Yao HJ, Sun YM, Hou MD, Mo D, Wang ZG, Neumann R. Electrochemical fabrication of single-crystalline and polycrystalline Au nanowires: the influence of deposition parameters. *Nanotech.* 2006; **17(8)**: 1922-1926.
202. Li NC, Yu SF, Harrell CC, Martin CR. Conical nanopore membranes- Preparation and transport properties. *Anal. Chem.* 2004; **76(7)**: 2025-2030.
203. Demoustier-Champagne S, Delvaux M. Preparation of polymeric and metallic nanostructures using a template-based deposition method. *Mater. Sci. Eng. C* 2001; **15(1-2)**: 269-271.
204. Brunetti B, Ugo P, Moretto LM, Martin CR. Electrochemistry of phenothiazine and methylviologen biosensor electron transfer mediators at nanoelectrode ensembles. *J. Electroanal. Chem.* 2000; **491(1-2)**: 166-174.
205. Crowley TA, Ziegler KJ, Lyons DM, Erts D, Olin H, Morris MA, Holmes JD. Synthesis of metal and metal oxide nanowire and nanotube arrays within a mesoporous silica template. *Chem. Mater.* 2003; **15(18)**: 3518-3522.
206. Ugo P, Pepe N, Moretto LM, Battagliarin M. Direct voltammetry of cytochrome c at trace concentrations with nanoelectrode ensembles. *J. Electroanal. Chem.* 2003; **560**: 51-58.
207. Moretto LM, Pepe N, Ugo P. Voltammetry of redox analytes at trace concentrations with nanoelectrode ensembles. *Talanta* 2004; **62(5)**: 1055-1060.
208. De Leo M, Kuhn A, Ugo P. 3D-ensembles of gold nanowires: preparation, characterization and electroanalytical peculiarities. *Electroanalysis* 2007; **19(2-3)**: 227-236.
209. Pereira FC, Moretto LM, De Leo M, Boldrin Zanoni MV, Ugo P. Gold nanoelectrode ensembles for direct trace electroanalysis of iodide. *Anal. Chim. Acta* 2006; **575(1)**: 16-24.
210. Savage J. *Handbook of Thick Film Technology*. Holmes PJ, Loasby RG eds. Electrochem. Publications Lim.; 1976. **Ch. 3**: 50.
211. White NM. *Thick Film Technology*. In: Prudenziati M editor. *Thick Film Sensors*, handbook of *Sens. & Act.* Amsterdam: Elsevier publ.; 1994. **Sec.1**: 3.
212. Vastarella W, Lanza B, Masci A, Pilloton R. Screen printed electrodes for biosensor application: reproducibility, sensitivity and stability. In: Di Natale C, D'Amico A, Martinelli G, Carotta MC, Guidi V eds. *Proceedings of the 9<sup>th</sup> Italian Conference on Sensor and Microsystems (AISEM)*, Ferrara (IT); 2004 Feb 8-11; ISBN 981-256-386-5; Singapore: World Scientific Publishing Co. Pte. Ltd; 2005: 19.
213. Delvaux M, Demoustier-Champagne S. Immobilisation of glucose oxidase within metallic nanotubes arrays for application to enzyme biosensors. *Bios. and Bioelectronics* 2003; **18(7)**: 943-951.
214. Delvaux M, Demoustier-Champagne S, Walcarius A. Flow injection amperometric detection at enzyme-modified gold nanoelectrodes. *Electroanalysis* 2004; **16(3)**: 190-198.

215. Maly J, Ilie M, Foglietti V, Cianci E, Minotti A, Nardi L, Masci A, Vastarella W, Pilloton R. Continuous flow micro-cell for electrochemical addressing of engineered bio-molecules. *Sensors and Actuators B* 2005; **111/112**: 317-322.
216. Zotti G, Cattarin S, Comisso N. Electrodeposition of polythiophene, polypyrrole and polyaniline by the cyclic potential sweep method. *J. Electroan. Chem.* 1987; **235(1-2)**: 259-273.
217. Andrade GD, Aguirre MJ, Biaggio SR. Influence of the first potential scan on the morphology and electrical properties of potentiodynamically grown polyaniline films. *Electroch. Acta* 1998; **44(4)**: 633-642.
218. Chowdhury AN, Ferdousi S, Islam MM, Okajama T, Ohsaka T. Arsenic detection by nanogold/conducting polymer-modified glassy carbon electrodes. *J. Appl. Pol. Sci.* 2007; **104(2)**: 1306-1311.
219. a) Swoboda B, Massey V. Properties of native glucose oxidase. *J. Biol. Chem.* 1965; **240**: 2209;  
b) Rodriguez-Nogales JM. Kinetic behaviour and stability of glucose oxidase entrapped in liposomes. *J. Chem. Tech. Biotech.* 2004; **79(1)**: 72-78.
220. Meier PC, Zund RE. *Statistical Methods in Analytical Chemistry*. In: Winefordner JD ed. *Chemical Analysis*. New York: J. Wiley & Sons Inc.; 1993. **123**: 87.
221. Thevenot DR, Toth K, Durst RA, Wilson GS. Electrochemical biosensors: recommended definitions and classification. *Bios. and Bioelectronics* 2001; **16(1-2)**: 121-131.
222. Thevenot DR, Toth K, Durst RA, Wilson GS. Electrochemical biosensors: recommended definitions and classification. *Anal. Letters* 2001; **34(5)**: 635-659.